Blumenols as shoot markers of root symbiosis with arbuscular mycorrhizal fungi

Ming Wang[1#], Martin Schäfer[1#ǂ], Dapeng Li[1], Rayko Halitschke[1], Chuanfu Dong[2Ɣ], Erica McGale[1], Christian Paetz[3], Yuanyuan Song[1†], Suhua Li[1], Junfu Dong[1,4], Sven Heiling[1‡], Karin Groten[1], Philipp Franken[5,6], Michael Bitterlich[7], Maria Harrison[8], Uta Paszkowski[9] and Ian T. Baldwin[1]*

[1] Max Planck Institute for Chemical Ecology, Department of Molecular Ecology, Hans Knöll Str. 8, 07745 Jena, Germany.

[2] Max Planck Institute for Chemical Ecology, Department of Bioorganic Chemistry, Hans Knöll Str. 8, 07745 Jena, Germany.

[3] Max Planck Institute for Chemical Ecology, Research Group Biosynthesis / NMR, Hans Knöll Str. 8, 07745 Jena, Germany.

[4] College of Life Sciences, University of Chinese Academy of Sciences, 101408 Beijing, China

[5] Leibniz-Institute of Vegetable and Ornamental Crops Großbeeren/Erfurt e.V, Kühnhäuser Str. 101, 99090 Erfurt, Germany

[6] Humboldt Universität zu Berlin, Institute of Biology, Philippstr. 13, 10115 Berlin, Germany.

[7] Leibniz-Institute of Vegetable and Ornamental Crops Großbeeren/Erfurt e.V, Theodor-Echtermeyer-Weg 1, 14979 Großbeeren, Germany.

[8] Boyce Thompson Institute for Plant Research, Tower Road, Ithaca, New York 14853, USA.

[9] University of Cambridge, Department of Plant Sciences, Street Downing, Cambridge CB2 3EA, United Kingdom.

[ǂ] Current address: University of Münster, Institute for Evolution and Biodiversity, Huefferstr. 1, 48149 Münster, Germany

[Ɣ] Current address: Max Planck Institute for Developmental Biology, Department of Integrative Evolutionary Biology, Max-Planck-Ring 1, 72076 Tübingen, Germany

[†] Current address: College of crop science, Fujian Agriculture and Forestry University, China

[‡] Current address: Institute of Clinical Chemistry and Laboratory Diagnostics and integrated Biobank Jena, Jena University Hospital, Am Klinikum 1, 07747 Jena, Germany

[#] Equal contribution

E-mail addresses: MW: mwang@ice.mpg.de, MS: mschaefer@ice.mpg.de, DL: dli@ice.mpg.de, RH: rhalitschke@ice.mpg.de, CD: chuanfu.dong@tuebingen.mpg.de, EM: emcgale@ice.mpg.de, CP: cpaetz@ice.mpg.de, YS: yyuansong@163.com, SL: sli@ice.mpg.de, JD: jdong@ice.mpg.de, SH: sheiling@ice.mpg.de, KG: kgroten@ice.mpg.de, PF: Franken@erfurt.igzev.de, MB: Bitterlich@igzev.de, MH: mjh78@cornell.edu, UP: up220@cam.ac.uk, ITB: baldwin@ice.mpg.de.

Running title: Leaf markers indicative of mycorrhization.

* Correspondence: Ian T. Baldwin, Department of Molecular Ecology, Max Planck Institute for Chemical Ecology. Hans-Knöll-Straße 8, 07745 Jena, Germany. E-mail: baldwin@ice.mpg.de

Abstract

High-through-put (HTP) screening for functional arbuscular mycorrhizal fungi (AMF)-associations is challenging because roots must be excavated and colonization evaluated by transcript analysis or microscopy. Here we show that specific leaf-metabolites provide broadly applicable accurate proxies of these associations, suitable for HTP-screens. With a combination of untargeted and targeted metabolomics, we show that shoot accumulations of hydroxy- and carboxyblumenol C-glucosides mirror root AMF-colonization in *Nicotiana attenuata* plants. Genetic/pharmacologic manipulations indicate that these AMF-indicative foliar blumenols are synthesized and transported from roots to shoots. These blumenol-derived foliar markers, found in many di- and monocotyledonous crop and model plants (*Solanum lycopersicum, Solanum tuberosum, Hordeum vulgare, Triticum aestivum, Medicago truncatula* and *Brachypodium distachyon*), are not restricted to particular plant-AMF interactions, and are shown to be applicable for field-based QTL mapping of AMF-related genes.

Introduction

More than 70% of all higher plants, including crop plants, form symbiotic associations with arbuscular mycorrhizal fungi (AMF) (Brundrett & Tedersoo, 2018). While the fungus facilitates the uptake of mineral nutrients, in particular phosphorous (P) and nitrogen, the plant supplies the fungus with carbon (Helber *et al.*, 2011; Bravo *et al.*, 2017; Jiang *et al.*, 2017; Keymer *et al.*, 2017; Luginbuehl & Menard, 2017). The interaction affects plant growth (Rooney *et al.*, 2009; Adolfsson *et al.*, 2015) and resistance to various abiotic and biotic stresses (Pineda *et al.*, 2010; Vannette *et al.*, 2013; Chitarra *et al.*, 2016; Sharma *et al.*, 2017). Although AMF interactions are physically restricted to the roots, they influence whole-plant performance, hence systemic metabolic responses have been anticipated, and searched for, but no general AMF-specific responses have been found (Bi *et al.*, 2007; Toussaint, 2007; Schweiger & Müller, 2015). While changes in foliar levels of carbohydrates, proteins, and amino acids, as well as secondary metabolites and phytohormones have been shown to respond to AMF inoculation (Schweiger *et al.*, 2014; Aliferis *et al.*, 2015; Adolfsson *et al.*, 2017), these changes are not specific to AMF interactions and tend to be general responses to various abiotic and biotic stresses. Moreover, these metabolic responses also tend to be taxa-specific, and many are likely indirect consequences of AMF-mediated effects on plant growth and development.

In contrast, large amounts of blumenol-type metabolites accumulate in roots after AMF inoculation. These compounds are apocarotenoids, in particular C_{13} cyclohexenone derivatives, produced by the cleavage of carotenoids. After AMF colonization, a C_{40} carotenoid is cleaved by carotenoid cleavage dioxygenase 7 (CCD7) to produce a C_{13} cyclohexenone and a C_{27} apocarotenoid which is further cleaved by CCD1 to yield a second C_{13} cyclohexenone (Floss *et al.*, 2008; Vogel *et al.*, 2010; Hou *et al.*, 2016). The compounds have been found to accumulate in the roots of AMF-colonized plants in a manner highly correlated with the fungal colonization rate (Fester *et al.*, 1999). Other stimuli such as pathogen infection and abiotic stresses, do not induce their accumulations (Maier *et al.*, 1997). The AMF-induced accumulation of these compounds is widespread and has been observed in roots of plant species from different families, including mono- and dicotyledons, (*Hordeum vulgare*, Peipp *et al.*, 1997; *Solanum lycopersicum* and *Nicotiana tobaccum*, Maier *et al.*, 2000; e.g., *Zea mays*, Fester *et al.*, 2002; *Lotus japonicus* and *Medicago truncatula*, Fester *et al.*, 2005; *Ornithogalum umbellatum*, Schliemann *et al.*, 2006; *Allium porrum*, Schliemann *et al.*, 2008).

Blumenols are classified into 3 major types; blumenol A, blumenol B and blumenol C (Figure 1A). However, previous studies have reported that only blumenol glycosides containing a blumenol C-based aglycone are positively correlated with mycorrhizal colonization. The aglycone can be additionally hydroxylated at the C11 or carboxylated at the C11 or C12 position (Maier *et al.*, 1997; Maier *et al.*, 2000). Additionally, 7,8-didehydro versions of blumenol C have been reported (Peipp *et al.*, 1997). The glycosylation usually occurs as an *O*-glycoside at the C9 position (Strack & Fester, 2006), but glycosylations at the hydroxylated C11 position have also been observed (Schliemann *et al.*, 2008). The glycosyl moiety can be a single sugar or

combinations of glucose (Glc), rhamnose, apiose, arabinose and/or glucuronic acid, which, in turn can be additionally malonylated or contain a 3-hydroxy-3-methylglutarate decoration (Strack & Fester, 2006; Schliemann *et al.*, 2008). The connections among sugar components can also vary (e.g., glucose-(1''→4')-glucose or glucose-(1''→6')-glucose; Maier *et al.*, 2000; Fester *et al.*, 2002). The particular type of decorations appears to be highly species-specific and it is likely that additional structural variants remain to be discovered. Exemplary structures are shown in Figure 1B.

Interestingly, blumenols such as blumenol A, blumenol A-9-*O*-Glc, blumenol B, blumenol C and blumenol C-9-*O*-Glc, were also reported to occur in the aerial parts of various plant species (Galbraith & Horn, 1972; Bhakuni *et al.*, 1974; Takeda *et al.*, 1997). However, most of these studies focused on the identification of natural products using large scale extractions (up to several kg of plant material) and were not performed in the context of AMF colonization. Furthermore, some blumenol compounds were also found in plant families that are known to have lost their ability to establish AMF interactions (Brassicaceae: Cutillo *et al.*, 2005; Urticaceae: Aishan *et al.*, 2010). These reports indicate AMF-independent constitutive levels of particular blumenols in aerial plant parts. Adolfsson *et al.* (2017) analyzed blumenol accumulations together with other metabolites in leaves of plants with and without AMF colonization. None of these studies reported AMF-specific accumulations of blumenols or transcripts specific for their biosynthesis. The concentrations of some blumenol derivatives were even reported to be down-regulated in response to AMF colonization (Adolfsson *et al.*, 2017).

The identification of a reliable metabolite marker in aerial plant tissues would be highly useful for AMF research since the characterization of AMF-associations is still laborious and time-consuming, typically requiring destructive root harvesting and microscopic examination or transcript analyses (Vierheilig *et al.*, 2005; Paradi *et al.*, 2010). To identify readily accessible AMF-indicative shoot metabolites, we hypothesized that a subset of the AMF-induced root metabolites would accumulate in shoots as a result of transport or systemic signaling.

Results

Blumenols are AMF-indicative metabolic fingerprints in roots

We performed an untargeted metabolomics analysis of root tissues in a transgenic line of *Nicotiana attenuata*, silenced in the calcium- and calmodulin-dependent protein kinase (ir*CCaMK*) and empty vector (EV) plants co-cultured with or without *Rhizophagus irregularis* (Figure 2A). By using ir*CCaMK* plants, unable to establish a functional AMF-association (Groten *et al.*, 2015), we were able to dissect the AMF association-specific metabolic responses from those changes that result from more general plant-fungus interactions. Untargeted metabolome profiling of roots using liquid chromatography (LC) coupled to time-of-flight mass spectrometry (qTOF-MS) resulted in a concatenated data matrix consisting of 943 mass features (*m/z* signals detected at particular retention times). A co-expression network analysis was conducted in which nodes represent *m/z* features and edges connect metabolite mass features originating from similar in-source fragmentations and sharing biochemical relationships (Li *et al.*, 2015; Li *et al.*, 2016). For example, features representing well-known compounds, like nicotine and phenylalanine, were tightly connected (Figure 2B). A STEM clustering pipeline was performed to recognize patterns of metabolite accumulations in the genotype × treatment data matrix [(EV/ir*CCaMK*) × (-/+ AMF inoculation)]. As a result, 5 of 8 computed distinct expression patterns were mapped onto the covariance network in Figure 2B (shown in different colors). A tightly grouped cluster of unknown metabolites, highlighted in red (Figure 2B) occupied a distinct metabolic space. Metabolites grouped in this cluster were highly elicited upon mycorrhizal colonization in EV, but not in ir*CCaMK* plants and not found in plants without AMF associations (Figure 2C). The structures of the compounds of this cluster were annotated based on tandem-MS and NMR data. Five metabolites were annotated as blumenols: 11-hydroxyblumenol C-9-*O*-Glc (Figure 2C; Compound 1), 11-carboxyblumenol C-9-*O*-Glc (Figure 2C; Compound 2), 11-hydroxyblumenol C-9-*O*-Glc-Glc (Compound 3), blumenol C-9-*O*-Glc-Glc (Compound 4) and blumenol C-9-*O*-Glc (Compound 5).

To quantify these compounds throughout the plant, we used a more sensitive and specifically targeted metabolomics approach based on LC-triple-quadrupole-MS. The abundance of the five blumenol C-glycosides continually increased with mycorrhizal development (Figure 2—figure supplement 1A) and was highly correlated with the mycorrhizal colonization rate as determined by the transcript abundances of classical arbuscular mycorrhizal symbiosis-marker genes (fungal house-keeping gene, *Ri-tub*; *plant* marker genes, *Vapyrin*, *RAM1*, *STR1* and *PT4;* Park *et al.* (2015); Figure 2—figure supplement 1B, Data Set 1).

Hydroxy- and carboxyblumenol C-glucoside levels in leaves positively correlate with root colonizations

Compounds 1 and 2 showed a similar AMF-specific accumulation in the leaves, as observed in the roots (Figure 2D). The other analyzed blumenols were not detected in leaves (Compounds 3 and 4; Figure 3—figure supplement 1A) or showed a less consistent AMF-specific accumulation (Compound 5; due to its constitutive background level; Figure 3—figure supplement 1A). The identity of Compounds 1 and 2 in the leaves was verified by high resolution qTOF-MS (Figure 3—figure supplement 1B-E).

Next, we determined the correlations between the contents of AMF-indicative foliar Compounds 1 and 2 and root colonization rates. In a kinetic experiment, the amount of both compounds steadily increased in the leaves of plants inoculated with *R. irregularis* (Figure 3A, Figure 3—figure supplement 2). At 3 wpi, the abundance of compounds 1 and 2 in the leaves was sufficient to reflect the colonization level of the roots. In contrast, the classical AMF-marker-genes, which are usually analyzed in the roots, did not respond in the leaves (Figure 4). In an inoculum-gradient experiment using increasing inoculum concentrations, proportionally higher Compound 1 and 2 levels were observed (Figure 3B), accurately reflecting the differential colonization of roots across treatments (Figure 3E). In addition to inoculation with a single AMF species (*R. irregularis*), we also tested mycorrhizal inoculum originally collected from the plant's native habitat, the Great Basin Desert in Utah, USA, which mainly consists of *Funneliformis mosseae* and *R. irregularis*. EV plants inoculated with this 'natural inoculum' also accumulated Compounds 1 and 2 in leaves, while ir*CCaMK* plants did not (Figure 3C). The analysis of a second independently transformed irCCaMK line confirmed the result that when the association with *R. irregularis* was genetically abrogated, Compounds 1 and 2 failed to accumulate in leaves of plants co-cultured with the AMF (Figure 3—figure supplement 3). When planted into the plant's natural environment in Utah, both EV and ir*CCaMK* plants could be clearly distinguished by their leaf Compound 1 and 2 contents. The signature of Compound 2 provided a better quality marker in these field-grown plants (Figure 3D, Figure 3—figure supplement 4). The foliar contents of these two compounds were highly correlated with the percentage of arbuscules in roots, the core structure of AMF interactions (Figure 3F, Figure 3—figure supplement 2). In contrast, other biotic or abiotic stresses, including herbivory, pathogen infection and drought stress, did not elicit the foliar accumulations of Compounds 1 and 2 (Figure 5). Such stimuli also do not induce blumenol accumulation in roots (Maier *et al.*, 1997). An analysis of various plant tissues, including different leaf positions, stem pieces, flowers and capsules revealed that these AMF-specific signatures accumulated throughout the shoot (Figure 3G). Taken together, we conclude that the contents of particular blumenols in aerial plant parts robustly reflect the degree of mycorrhizal colonization in *N. attenuata* plants.

AMF–indicative blumenols in shoots most likely originate from the roots

Blumenols are apocarotenoids originating from a side branch of the carotenoid pathway (Hou *et al.*, 2016). Most of the candidate genes for blumenol biosynthesis were upregulated in roots, but not in leaves of *N. attenuata* plants in response to mycorrhizal colonization (Figure 6A, Figure 6—figure supplement 1A). We inferred that these AMF-indicative leaf apocarotenoids are transported from their site of synthesis in colonized roots to other plant parts. This is consistent with the occurrence of blumenols in stem sap (Figure 6—figure supplement 1B) which was collected by centrifuging small stem pieces. To clarify the origins (local biosynthesis vs. transport) of these leaf blumenols, we genetically manipulated the carotenoid biosynthesis of *N. attenuata* plants. To minimize the effects of a disturbed carotenoid biosynthesis on the AMF-plant interaction, we used the dexamethasone (DEX)-inducible pOp6/LhGR system to silence phytoene desaturase (PDS) expression in a single DEX-treated leaf position (Schäfer *et al.*, 2013). Treated leaves showed clear signs of bleaching, indicating PDS silencing (Figure 6B, Figure 6—figure supplement 1C), but levels of the AMF-indicative Compounds 1 and 2 were not affected, consistent with their transport from other tissues, likely the highly accumulating roots. As a control, we analyzed the non-AMF-inducible Compound 6, showing constitutive levels in aerial tissues (Figure 6—figure supplement 2). In DEX-treated leaves, Compound 6 concentrations were reduced by nearly 40%, consistent with local production (Figure 6B, Figure 6—figure supplement 1D). To confirm the within-plant transport potential of blumenols, we dipped roots of seedlings into aqueous solutions of Compounds 1 or 2. After overnight incubation, the blumenol derivatives were clearly detected not only in roots, but also in shoots (Figure 6C, Figure 6—figure supplement 1E).

The analysis of AMF-indicative blumenols as HTP screening tool for forward genetics approaches

To test the potential of the foliar AMF-indicative metabolites as a screening tool, we quantified the concentration of Compounds 1 and 2 in leaves of plants of a population of recombinant inbred lines (RILs) of a forward genetics experiment, an experiment which would be challenging with the classical screening tools of root staining or nucleic acid analysis. We focused our analysis on Compound 2 due to the superior quality of its signature in the leaves of field-grown plants (Figure 3—figure supplement 4). The experiment consisted of a population of RILs from a cross of two *N. attenuata* accessions (Utah, UT and Arizona, AZ)(Zhou *et al.*, 2017) which differ in their mycorrhizal colonization (Figure 7A-B, Figure 7—figure supplement 1) and accumulation of foliar Compound 2 in the glasshouse (Figure 7C). A QTL analysis of 728 plants grown across a 7200 m^2 field plot (Figure 7D) revealed that the abundance of Compound 2 mapped to a single locus on linkage group 3 (Figure 7E), which harbored a homologue of *NOPE1*(*NIATv7_g02911*) previously shown to be required for the initiation of AMF symbioses in maize and rice (Nadal *et al.*, 2017). Transcripts of *NaNOPE1* were more abundant in AZ roots after AMF inoculation, but did not differ significantly in leaves (Figure 7—figure supplement

1B). While clearly requiring additional follow-up work, these results highlight the value of these signature metabolites for HTP screens, which form the basis of most crop improvement programs.

AMF-indicative blumenols in shoots are a widespread response of various plant species to different kinds of AMF

The AMF-specific accumulation of blumenol C-derivatives in roots is a widespread phenomenon within higher plants (Strack & Fester, 2006); however, how general are the observed blumenol changes in aerial parts across different combinations of plants and AMF species? We analyzed *Solanum lycopersicum*, *Triticum aestivum* and *Hordeum vulgare* plants with and without AMF inoculation and again we found an overlap in the AMF-specific blumenol responses in roots and leaves, consistent with the transport hypothesis. Further analyses led to the identification of additional AMF-indicative blumenols in the leaves of *Medicago truncatula*, *Solanum tuberosum* and *Brachypodium distachyon*. We identified various types of blumenols that showed an AMF-specific accumulation in the shoot, including blumenol B (Compound 7), which has not previously been reported in an AMF-dependent context (Figure 7F; Figure 7—figure supplement 2). As reported for roots, the particular blumenol types were species-dependent, but the general pattern was widespread across monocots and dicots in experiments conducted at different research facilities. In tests with diverse fungal species (*R. irregularis*, *F. mosseae* and *Glomus versiforme)*, the observed effects were not found to be restricted to specific AMF taxa (Figure 7F; Figure 7—figure supplement 2). In short, the method is robust.

Discussion

AMF-interactions are proposed to have played an important role for the colonization of land by plants and still play an important role for a majority of plants by improving the function of their roots and increasing whole-plant performance. Consequently, the investigation of AMF-mediated effects on a host plant's physiology has been an important research field for many decades and characteristic transcriptional and metabolic changes have been observed in the roots of AMF-colonized plants. However, the cumbersome analysis of AMF-interactions, involving destructive harvesting of root tissues and microscopic or transcript analysis, restrains large-scale investigations and commercial applications. AMF interactions were also shown to affect the primary and secondary metabolism in the systemic, aerial tissues of plants; however none of these responses proved to be widespread and sufficiently specific to function as reliable markers (Schweiger & Müller, 2015). Here we describe the discovery of particular blumenols as AMF-indicative markers in leaves and other systemic aerial tissues and illustrate their potential application as tools for research and plant breeding.

Systemic AMF-mediated metabolite changes

Metabolites and metabolite responses are often specific to particular parts and tissues of a plant (Li *et al.*, 2016; Lee *et al.*, 2017), but it is also known that local responses can spread to other plant parts. Additionally, metabolites do not only accumulate at their place of biosynthesis but can be readily transported throughout the plant (Baldwin, 1989). Therefore, we hypothesized that local changes in the roots might also be reflected in the systemic aerial tissues, either by signaling or transport. This allowed us to identify specific AMF-indicative blumenols in the shoot (Figure 3) despite the occurrence of other highly abundant and constitutively produced compounds and blumenols that are not indicative of AMF-associations. Interestingly, the confirmation of compound identities in leaf samples with high resolution MS techniques proved to be challenging and required additional sample purification steps. Likely, such matrix effects thwarted the detection of these AMF-indicative, systemic blumenol responses in previous investigations. Under our conditions, AMF-indicative blumenols began mirroring the colonization rates of roots at around 3 wpi (Figure 3—figure supplement 2). Although, microscopic methods can detect first signs of AMF colonization of the roots already after a few days (Brundrett *et al.*, 1985), the sensitivity of our method was found to be sufficient to analyze colonization rates observed in the glasshouse and, more importantly, in nature (Figure 3 and 7). The discovery of these AMF-indicative blumenol compounds in diverse plant species interacting with different AMF species (Figure 7, Figure 7—figure supplement 2) further indicates that these responses are widespread. AMF-induced blumenols in the roots have been shown to be quantifiable by various MS and photodiode array based detector setups. However, AMF-induced blumenols occur in many-fold lower amounts in the leaves compared to the roots (e.g., Compound 1 in *N. attenuata* approximately 1/10) and, at these low concentrations, their analysis is likely thwarted by complex matrix effects. Therefore, their analysis requires detection systems

with advanced sensitivity and selectivity as is offered by state-of-the-art triple quadrupole technology and enhanced sample preparations (e.g., by solid-phase-extraction based purification and concentration) which were used in the quantitative detection of leaf blumenols described here. In addition to the blumenols, mycorradicin, another biosynthetically-related type of apocarotenoids, was reported to accumulate in AMF-colonized roots (Klingner *et al.*, 1995) and it would be interesting to investigate if mycorradicin accumulates throughout the plant, as well.

Root-to-shoot transport of AMF-indicative blumenols

Despite the AMF-induced accumulation of blumenols in the shoot, putative candidate genes of the apocarotenoid biosynthesis pathway were only induced in the roots of AMF-inoculated plants (Figure 6A, Figure 6—figure supplement 1A). To exclude other mechanisms (e.g., post-transcriptional regulation) mediating the local production of the blumenol compounds in the leaves, we genetically manipulated the carotenoid pathway in a tissue-specific manner. It is challenging to manipulate blumenols without affecting the AMF-colonization of the plant, since other carotenoid-derived compounds, such as strigolactones, are known to play an important role in this process (Lanfranco *et al.*, 2017). To circumvent these problems, we used the LhGR/pOp6 system for chemically-inducible RNAi-mediated gene silencing of PDS (Schäfer *et al.*, 2013) to impair carotenoid biosynthesis only in a particular leaf of AMF-inoculated plants. Interestingly, only the constitutively produced Compound 6 was reduced in the treated leaves, while the AMF-indicative Compounds 1 and 2 were not affected by our treatment (Figure 6B). This indicated that instead of being locally produced, Compound 1 and 2 are translocated from the roots, an inference consistent with the occurrence of AMF-indicative blumenols in stem sap and the capacity of seedlings to transport blumenols from the root to the shoot from hydroponic solution (Figure 6C, Figure 6—figure supplement 1B, D). It seems likely that the AMF-indicative blumenols are transported in the xylem with the transpiration stream (Figure 6D). The blumenol glucosides (Compounds 1, 2 and 6) are hydrophilic low-molecular weight (402, 388 and 386 Da), compounds that are unlikely to pass membranes without further support, e.g., by transporters. It was recently demonstrated that ATP-binding cassette (ABC) transporters (G-type) are involved in the root-to-shoot transport of ABA, a phytohormone with a molecular structure related to blumenols, and these transporters resemble the function of other ABCG-type proteins reported to mediate the long-distance transport of cytokinins and strigolactones (Borghi *et al.*, 2015). Whether blumenols are transported by similar mechanisms remains an interesting question.

Functional implication of blumenol accumulation and transport

Blumenols were shown to accumulate in large amounts in the roots of various plants after AMF-inoculation (Strack & Fester, 2006) and our data indicate that they are subsequently distributed throughout the plant (Figure 3G). While the conservation of this response in various plants after inoculation with different AMF species (Figure 7F, Figure 7—figure supplement 2) indicates an

important functional role in the AMF-plant interaction, this function remains to be explored. Unfortunately, the current knowledge of the biological activity of blumenols only vaguely indicates potential systemic functions of AMF-induced blumenols in shoot tissues. Activity studies on vomifoliol, the aglycone of the not AMF-indicative Compound 6, showed that this compound induces stomatal closure similar to the structurally related abscisic acid (Stuart & Coke, 1975). Additionally, blumenols are known to suppress seed germination and plant growth (Kato-Noguchi *et al.*, 2012; Kato-Noguchi *et al.*, 2015). Therefore, AMF-induced blumenols could serve as systemic signals that mediate the large-scale adjustments in general physiology that are thought to accompany AMF-interactions. For example, AMF-induced blumenols could be involved in the regulation of differential susceptibility of AMF-inoculated plants to stresses, such as drought or pathogen infection.

AMF-indicative blumenols as tool for research and plant breeding

Even if classical tools for the quantification of AMF-plant interactions can offer superior sensitivity they are labor intensive and highly destructive which limits their application in studies that require high sample throughput, as well as in experiments that require repeated analysis of plants. We propose that the analysis of AMF-indicative blumenols in the shoot provides a convenient, easy-to-use, and minimally destructive tool to interrogate plant-AMF interactions in a HTP manner that allows for forward genetic studies even under field conditions (Figure 7E) and empowers plant breeding programs to produce mycorrhiza-responsive and P-efficient high-yielding lines (van de Wiel *et al.*, 2016). Currently, phosphate fertilizer is derived from phosphate rock, a non-renewable resource, which is predicted to be depleted soon (Vaccari & Strigul, 2011). By enabling breeding programs to select crop varieties which have negotiated AMF symbioses that deliver high yields with minimal P inputs, this discovery could help steer the “green revolution” away from intense agricultural inputs and the collateral environmental damage they cause. While some of the “green revolution” crop varieties with gibberellin response defects are potentially more efficient in Pi uptake as a result of their higher root colonization rates by AMF (Floss *et al.*, 2013; Foo *et al.*, 2013) this serendipitous breeding event underscores the value of explicitly designing crop breeding programs to produce crops that negotiate more favorable AMF associations.

Materials and Methods

Key resources table

Reagent type (species) or resource	Designation	Source or reference	Additional information
genetic reagent (*N. attenuata*)	A-09-1212-1	Groten et al., 2015, DOI: 10.1111/pce.12561	stably silenced in CCaMK via RNAi
genetic reagent (*N. attenuata*)	A-09-1208-6	Groten et al., 2015, DOI: 10.1111/pce.12561	stably silenced in CCaMK via RNAi
genetic reagent (*N. attenuata*)	A-11-92-4 × A-11-325-4	Schäfer et al., 2013, DOI: 10.1111/tpj.12301	chemically-inducible silenced in PDS via RNAi
genetic reagent (*N. attenuata*)	A-04-266-3	Bubner et al., 2006, DOI: 10.1007/s00299-005-0111-4	empty vector control
biological sample (*N. attenuata*)	AZ-UT RIL	Zhou et al., 2017, DOI: 10.1016/j.cub.2017.03.017	biparental QTL mapping population

Plant material and AMF inoculation

For our experiments with *Nicotiana attenuata* (Torr. ex S. Wats.), we used plants from the 31st inbred generation of the inbred 'UT' line, ir*CCaMK* [A-09-1208-6 and A-09-1212-1(Groten *et al.*, 2015)] plants that are stably silenced in *CCaMK* via RNAi, i-ir*PDS* plants (A-11-92-4 × A-11-325-4; Schäfer *et al.*, 2013) harboring the LhGR/pOp6 system for chemically-inducible RNAi-mediated gene silencing of phytoene desaturase (PDS) and the respective empty vector (EV) transformed plants (A-04-266-3; Bubner *et al.*, 2006) as controls. Details about the transformation and screening of the ir*CCaMK* plants are described by Groten *et al.* (2015) and for the i-ir*PDS* plants by Schäfer *et al.* (2013). Seeds were germinated on Gamborg B5 as described by Krügel *et al.* (2002). The advance intercross recombinant inbred line (RIL) population was developed by crossing two *N. attenuata* inbred lines originating from accessions collected in Arizona (AZ) and Utah (UT), USA (Glawe *et al.*, 2003; Zhou *et al.*, 2017). Additionally, we used *Solanum lycopersicum* 'Moneymaker', *Hordeum vulgare* 'Elbany' and *Triticum aestivum* 'Chinese Spring' plants.

For glasshouse experiments, plants were treated according to Groten *et al.* (2015). In brief, they were transferred into dead (autoclaved twice at 121 °C for 30 min; non-inoculated controls) or living inoculum (*R. irregularis*, Biomyc Vital, inoculated plants) diluted 1:10 with expanded clay (size: 2–4 mm). Pots were covered with a thin layer of sand. Plants were watered with distilled water for 7 d and subsequently fertilized every second day either with a full strength hydroponic solution (for 1 L: 0.1292 g $CaSO_4 \times 2H_2O$, 0.1232 g $MgSO_4 \times 7H_2O$, 0.0479 g K_2HPO_4, 0.0306 g KH_2PO_4, 2mL KNO_3 (1 M), 0.5 mL micronutrients, 0.5 mL Fe diethylene triamine pentaacetic acid) or with a low P hydroponics solution containing only 1/10 of the regular P-concentration (0.05 mM). Plants were grown separately in 1L pots, if not stated otherwise. In the paired design (Figure 2), ir*CCaMK* plants were grown together with EV plants

in 2L pots and the watering regime was changed to ¼ of the regular P-concentration after plants started to elongate. Glasshouse experiments with natural inoculum (Figure 3C) were conducted in a mesocosm system (4 boxes, each 2 pairs of EV and ir*CCaMK* plants). Plants were maintained under standard glasshouse conditions (16 h light, 24-28 °C, and 8 h dark, 20- 24 °C and 45 -55% humidity) with supplemental light supplied by high-pressure sodium lamps (Son-T-Agro).

The field experiments were conducted as described by Schuman *et al.* (2012). Seedlings were transferred to Jiffy pots and planted into a field plot at the Lytle Ranch Preserve in the Great Basin Desert (Utah, USA: N 37.1412, W 114.0275). Field season 2016 (Figure 3D): field experiments were conducted under the US Department of Agriculture Animal and Plant Health Inspection Service (APHIS) import permission numbers 10-004-105m (ir*CCaMK*) and 07-341-101n (EV) and the APHIS release permission number 16-013-102r. EV and ir*CCaMK* plants were planted in communities of six plants, either of the same genotype or with both genotypes in equal number.

Sample collection

During harvests, roots were washed and briefly dried with a paper towel. Subsequently, they were cut into 1 cm pieces and mixed. Plant tissues were shock-frozen in liquid nitrogen immediately after collection, ground to a fine powder and stored at -20°C (short-term storage)/-80°C (long-term storage) until extraction. From the root samples, an aliquot was stored in root storage solution (25% ethanol and 15% acetic acid in water) at 4 °C for microscopic analysis.

For stem sap collection, branches of *N. attenuata* plants were cut into 1.5cm long pieces and placed into small 0.5 mL reaction tubes with a small hole in the tip, which were placed in a larger 1.5 mL reaction tube. The tubes were centrifuged for 15 min at 10 000 × g. The stem sap from the larger reaction tubes was collected and stored at -20°C.

Samples prepared at other laboratory facilities

Medicago truncatula (Figure 7 and Figure 7—figure supplement 2) and *Brachypodium distachyon* (Figure 7 and Figure 7—figure supplement 2) samples were prepared at the laboratory of Prof. Maria Harrison from the Boyce Thompson Institute for Plant Research (Ithaca, NY, USA). *M. truncatula* plants were grown in a growth chamber with a 16 h light (25°C)/8 h dark (22°C) cycle. *B. distachyon* plants were grown in growth chamber with a 12 h light (24 ºC) / 12 h dark (22 ºC) cycle. All experiments were carried out in surface sterilized containers, autoclaved growth substrates and with surface sterilized spores and seeds as described previously (Liu *et al.*, 2004; Hong *et al.*, 2012; Floss *et al.*, 2013). The growth substrates were mixtures of play sand (average particle 200-300 µm), black sand (heterogeneous particle size 50 – 300 µm) and gravel (heterogeneous particle size 300 µm -10 mm) as outlined below. For *M. truncatula*, 2 d-old seedlings were planted into 20.5 cm cones (Cone-tainers) containing a 1:1 mixture of sterile black sand and gravel with 200 surface-sterilized *G.*

versiforme spores placed on a layer of play sand positioned 4 cm below the top of the cones. Five seedlings were planted into each cone. Plants were fertilized twice weekly with 20 mL of with modified 1/2-strength Hoagland's solution (Millner & Kitt, 1992) containing 100 µM potassium phosphate. Plants were harvested 49 d post planting and tissue frozen in liquid nitrogen and stored at -80 C. One cone containing 5 seedlings represents one biological replicate. The harvest date was 3/3/2015. *B. distachyon* seedlings were planted into cones (Cone-tainers) containing a 2:1:1 mixture of black sand:play sand:gravel with 300 surface-sterilized *G. versiforme* spores placed on a layer of play sand positioned 4 cm below the top of the cones. Plants were fertilized twice weekly with 20 mL of modified 1/4-strength Hoagland's solution (Millner & Kitt, 1992) containing 20 µM potassium phosphate. Plants were harvested 35 d post planting and tissue frozen in liquid nitrogen and stored at -80 C. Each cone contained 3 plants and each biological replicate consisted of a pool of 4 cones. The harvest date was 6/20/2016.

S. lycopersicum 'Moneymaker' (Figure 7—figure supplement 2) and *Solanum tuberosum* 'Wega' (Figure 7) samples were prepared at the laboratory of Prof. Philipp Franken by Dr. Michael Bitterlich from the Leibniz-Institute of Vegetable and Ornamental Crops (Großbeeren/Erfurt Germany). *S. lycopersicum* were transplanted into 10 L open pots containing a sand/vermiculite mixture (sand: grain size 0.2–1 mm; Euroquarz, Ottendorf-Okrilla, Germany, vermiculite:agra vermiculite, Pullrhenen, Rhenen, The Netherlands; 1:1 v:v) and grown in the glass house from March to May (20-28:17°C day:night, PAR: 300-2000 µmol m^{-2} s^{-1}). Mycorrhizal plants were inoculated with a commercial inoculum either containing *R. irregularis* DAOM 197198 (INOQ, Schnega, Germany) or *F. mosseae* BEG12 (MycAgro Laboratory, Breteniere, France) with 10 % of the substrate volume and were harvested after 11 or 6 weeks, respectively. *S. tubersosum* tubers of similar size were planted into 3 L pots filled with the same substrate and grown in a growth cabinet (20:16°C day:night, 16 h light, 8 h dark; PAR: 250-400 µmol m^{-2} s^{-1}, 50 % rH). Mycorrhizal plants were inoculated with a commercial inoculum containing *F. mosseae* BEG12 (MycAgro Laboratory, Breteniere, France) with 10 % of the substrate volume and were harvested after 6 weeks. Non-mycorrhizal counterparts were inoculated with the same amount of autoclaved (2 h, 121°C) inoculum and a filtrate. The filtrate was produced for every pot by filtration of 200 mL deionized water through Whatman filter (particle retention 4–7 µm; GE Healthcare Europe GmbH, Freiburg, Germany) containing approx. 200 mL of inoculum. The same amount of deionized water (200 mL) was added to mycorrhizal pots. Plants were irrigated every other day with 400- 600 mL nutrient solution (De Kreij *et al.*, 1997); 40% of full strength) with 10% of the standard phosphate to guarantee good colonization (N:10.32 mM; P: 0.07 mM, K: 5.5 mM, Mg: 1.2 mM, S: 1.65 mM, Ca: 2.75 mM, Fe: 0.02 mM, pH: 6.2, EC: 1.6 mS). For the experiment in the glasshouse, additional irrigation was carried out with deionized water until pot water capacity every other day. The pooled bulk leaf sample was dried at 60°C for 48 h, ground to a fine powder and stored under dry conditions at room temperature until further analyses.

Stress treatments

Herbivory treatments were conducted by placing *Manduca sexta* neonates, originating from an in-house colony, on the plants. After feeding for 2 weeks, rosette leaves were harvested. As controls, we harvested leaves from untreated plants.

For bacteria and virus infection, plants were inoculated with *Agrobacterium tumefaciens* carrying the Tobacco Rattle Virus. The inoculation was conducted by infiltrating leaves with a bacteria suspension using a syringe. The treatment was conducted as described for virus-induced gene silencing described by Ratcliff *et al.* (2001) and by Saedler and Baldwin (2004). After incubation for 3 weeks, stem leaves of the treated plants and untreated control plants were harvested.

The fungal infection was done with *Botrytis cinerea*. On each plant, three leaves were treated by applying 6 droplets each containing 10 µL of *B. cinerea* spore suspension (10^6 spores mL^{-1} in Potato Extract Glucose Broth, Carl Roth GmbH) to the leaf surface. As control, plants were treated with broth without spores in the same way. Samples were collected after 4 days incubation.

Drought stress was induced by stopping the watering for 4 d. Subsequently, stem leaves of the drought-stressed plants and the continuously watered control plants were harvested. In contrast to the other samples of the stress experiment, leaves were dried before analysis to compensate for weight differences caused by changes in the water content.

Sample preparation - extraction and purification

For extraction, samples were aliquoted into reaction tubes, containing two steel balls. Weights were recorded for later normalization. Per 100 mg plant tissues (10 mg in case of dry material), approximately 1 mL 80% MeOH was added to the samples before being shaken in a GenoGrinder 2000 (SPEX SamplePrep) for 60 s at 1150 strokes min^{-1}. After centrifugation, the supernatant was collected and analyzed. For triple-quadrupole MS quantification, the extraction buffer was spiked with stable isotope-labeled abscisic acid (D_6-ABA, HPC Standards GmbH) as an internal standard.

Stem sap was diluted 1:1 with MeOH spiked with D_6-ABA as an internal standard. After centrifugation, the supernatant was collected and analyzed.

The purification of *N. attenuata* leaf extracts for high resolution qTOF-MS was conducted by solid-phase-extraction (SPE) using Chromabond HR-XC 45 µm benzensulfonic acid cation exchange columns (Machery-Nagel) to remove abundant constituents, such as nicotine and phenolamides. After purification the samples were evaporated to dryness and reconstituted in 80% methanol.

Compound identification was conducted by NMR with purified fractions of root and leaf extracts. Compounds 1, 3 and 4 were extracted from root tissues of *N. attenuata* and purified by HPLC (Agilent-HPLC 1100 series; Grom-Sil 120 ODS-4 HE, C18, 250 × 8 mm, 5 µm; equipped with a Gilson 206 Abimed fraction collector). Compounds 2 and 7 were extracted from a mixture of leaf tissues from different plant species (*M. truncatula, Z. mays, S. lypersicum* and *N.*

attenuata). The first purification step was conducted by SPE using the Chromabond HR-XC 45 µm benzensulfonic acid cation exchange columns (Machery-Nagel) to remove hydrophilic and cationic constituents. Additional purification steps were conducted via HPLC (Agilent-HPLC 1100 series; Phenomenex Luna C18(2), 250 × 10 mm, 5 µm; equipped with a Foxy Jr. sample collector) and UHPLC (Dionex UltiMate 3000; Thermo Acclaim RSLC 120 C18, 150 × 2.1 mm, 2.2 µm; using the auto-sampler for fraction collection).

Untargeted MS based analyses

For high resolution mass spectrometry (MS), indiscriminant tandem mass spectrometry (idMS/MS), tandem MS (MS^2) and pseudo-MS^3 were used. Ultra-high performance liquid chromatography (UHPLC) was performed using a Dionex UltiMate 3000 rapid separation LC system (Thermo Fisher), combined with a Thermo Fisher Acclaim RSLC 120 C18, 150 × 2.1 mm, 2.2 µm column. The solvent composition changed from a high % A (water with 0.1% acetonitrile and 0.05% formic acid) in a linear gradient to a high % B (acetonitrile with 0.05 % formic acid) followed by column equilibration steps and a return to starting conditions. The flow rate was 0.3 mL/min. MS detection was performed using a micrOTOF-Q II MS system (Bruker Daltonics), equipped with an electrospray ionization (ESI) source operating in positive ion mode. ESI conditions for the micrOTOF-Q II system were end plate offset 500 V, capillary voltage 4500 V, capillary exit 130 V, dry temperature 180°C and a dry gas flow of 10 L min^{-1}. Mass calibration was performed using sodium formiate (250 mL isopropanol, 1 mL formic acid, 5 mL 1 M NaOH in 500 mL water). Data files were calibrated using the Bruker high-precision calibration algorithm. Instrument control, data acquisition and reprocessing were performed using HyStar 3.1 (Bruker Daltonics).

idMS/MS was conducted in order to gain structural information on the overall detectable metabolic profile. For this, samples were first analyzed by UHPLC-ESI/qTOF-MS using the single MS mode (producing low levels of fragmentation that resulted from in-source fragmentation) by scanning from m/z 50 to 1400 at a rate of 5000 scans/s. MS/MS analyses were conducted using nitrogen as collision gas and involved independent measurements at the following 4 different collision-induced dissociation (CID) voltages: 20, 30, 40 and 50 eV. The quadrupole was operated throughout the measurement with the largest mass isolation window, from m/z 50 to 1400. Mass fragments were scanned between m/z 50 to 1400 at a rate of 5000 scans/s. For the idMS/MS assembly, we used a previously designed precursor-to-product assignment pipeline (Li *et al.*, 2015; Li *et al.*, 2016) using the output results for processing with the R packages XCMS and CAMERA (Data Set 2).

Additional MS/MS experiments were performed on the molecular ion at various CID voltages. For the fragmentation of the proposed aglycones via pseudo-MS^3, we applied a 60 eV in-source-CID transfer energy which produced spectra reflecting the loss of all sugar moieties.

Structure elucidation by NMR

Purified fractions were completely dried with N_2 gas and reconstituted with MeOH-d_3 prior to analysis by nuclear magnetic resonance spectroscopy (NMR). Structure elucidation was accomplished on an Avance III AV700 HD NMR spectrometer (Bruker-Biospin, Karlsruhe, Germany) at 298 K using a 1.7 mm TCI CryoProbe™ with standard pulse programs as implemented in Bruker TopSpin (Version 3.2). Chemical shift values (δ) are given relative to the residual solvent peaks at δ_H 3.31 and δ_C 49.05, respectively. Carbon shifts were determined indirectly from ^{1}H-^{13}C HSQC and ^{1}H-^{13}C HMBC spectra. The data are shown in Table 1 and compared the results with previously published reference data (Matsunami *et al.*, 2010). Blumenol C glucoside and byzantionoside B differ only in the configuration of position C-9; blumenol C glucoside is (9*S*)-configured whereas byzantionoside B has (9*R*)-configuration. Characteristic ^{13}C-chemical shift differences can thus be found for the positions C-9, C-10 and C-1'. In byzantionoside, C-9 and C-10 were reported to have chemical shifts of δ_C 75.7 and δ_C 19.9, respectively. In contrast, the chemical shifts for the same positions in blumenol C glucoside were reported to be lowfield shifted to δ_C 77.7 and δ_C 22.0, respectively. Experimental chemical shifts of C-9 for the compounds identified in this publication were in the range from δ_C 77.2 to δ_C 78.2, and for C-10 in the range from δ_C 21.6 to δ_C 21.9, respectively. C-1' of byzantionoside was reported to have a chemical shift of δ_C 102.3, while for blumenol C glucoside the chemical shift was δ_C 104.1. The experimental chemical shifts for C-1' of the compounds of this publication are in the range from δ_C 103.8 to δ_C 104.1. Hence the ^{13}C-chemical shift data are completely consistent with the structures being blumenol C glucosides rather than byzantionoside B. More characteristic differences can be found in the ^{1}H chemical shifts. The methylene shifts for H-7 of byzantionoside were reported to have chemical shifts of δ_H 1.50 and δ_H 1.98 while for blumenol C glucoside the same position showed chemical shifts of δ_H 1.67 and δ_H 1.81. Experimental ^{1}H chemical shifts for H-7 of the compounds 1-4 of this publication were found in the range of δ_H 1.62 to δ_H 1.69 and δ_H 1.80 to δ_H 1.88, respectively. Consequently, the NMR data clearly establish the structures to be blumenol C derivatives and not byzantionosides.

Targeted metabolite analysis

For chromatographic separations, a UHPLC (Dionex UltiMate 3000) was used to provide a maximum of separation with short run times. This reduced the interference from other extract components (matrix effects), increased the specificity of the method, and met the requirements of a HTP analysis. The auto-sampler was cooled to 10°C. As a stationary phase, we used a reversed phase column (Agilent ZORBAX Eclipse XDB C18, 50 × 3.0 mm, 1.8 µm) suitable for the separation of moderately polar compounds. Column temperature was set to 42°C. As mobile phases, we used: A, 0.05% HCOOH, 0.1% ACN in H_2O and B, MeOH, the composition of which was optimized for an efficient separation of blumenol-type compounds within a short run time. We included in the method a cleaning segment at 100% B and an equilibration segment allowing for reproducible results across large samples sets. The gradient program was as follows: 0–1 min, 10% B; 1–1.2 min, 10-35% B; 1.2–5 min, 35-50% B; 5–5.5 min, 50-100% B; 5.5–6.5

min, 100% B; 6.5–6.6 min, 100-10% B and 6.6–7.6 min, 10% B. The flow rate was set to 500 µL min^{-1}. Analysis was performed on a Bruker Elite EvoQ triple quadrupole MS equipped with a HESI (heated electrospray ionization) ion source. Source parameters were as follows: spray voltage (+), 4500V; spray voltage (-), 4500V; cone temperature, 350°C; cone gas flow, 35; heated probe temperature, 300°C; probe gas flow, 55 and nebulizer gas flow, 60. Samples were analyzed in multi-reaction-monitoring (MRM) mode; the settings are described in Table 2.

Method for targeted blumenol analysis in *N. attenuata*

The compound list was limited to the AMF-indicative markers in *N. attenuata*, Compound 1 and 2, the not AMF-indicative Compound 6 and the internal standard (D_6-ABA). Accordingly, the gradient program was adjusted as follows: 0–1 min, 10% B; 1–1.2 min, 10-35% B; 1.2–3 min, 35-42% B; 3–3.4 min, 42-100% B; 3.4–4.4 min, 100% B; 4.4–4.5 min, 100-10% B and 4.5–5.5 min, 10% B. The MRM settings are given in Table 3.

Determination of the AMF colonization rate

To determine the fungal colonization rates and mycorrhizal structures, root samples were stained and analyzed by microscopy. For WGA-Alexa Fluor 488 staining, roots were first washed with distilled water and then soaked in 50% (v/v) ethanol overnight. Roots were then boiled in a 10% (w/v) KOH solution for 10 minutes. After rinsing with water, the roots were boiled in 0.1 M HCl solution for 5 minutes. After rinsing with water and subsequently with 1x phosphate-buffered saline solution, roots were stained in 1x phosphate-buffered saline buffer containing 0.2 mg mL^{-1} WGA-Alexa Fluor 488 overnight in the dark. Zeiss confocal microscopy (LSM 510 META) was used to detect the WGA-Alexa Fluor 488 (excitation/emission maxima at approximately 495/519 nm) signal. Trypan blue staining was performed as described by Brundrett *et al.* (1984) to visualize mycorrhizal structures. For the counting of mycorrhizal colonization, 15 root fragments, each about 1 cm long, were stained with either trypan blue or WGA-488 followed by slide mounting. More than 150 view fields per slide were surveyed with 20x object magnification and classified into 5 groups: no colonization, only hyphae (H), hyphae with arbuscules (H+A), hyphae with vesicles (V+H), and hyphae with arbuscules and vesicles (A+V+H). The proportions of each group were calculated by numbers of each group divided by total views.

For the molecular biological analysis of colonization rates, RNA was extracted from the roots using the RNeasy Plant Mini Kit (Qiagen) or NucleoSpin® RNA Plant (Macherey-Nagel) according to the manufacturer's instructions and cDNA was synthesized by reverse transcription using the PrimeScript RT-qPCR Kit (TaKaRa). Quantitative (q)PCR was performed on a Stratagene Mx3005P qPCR machine using a SYBR Green containing reaction mix (Eurogentec, qPCR Core kit for SYBR Green I No ROX). We analyzed the *R. irregularis* specific housekeeping gene, *Ri-tub* (GenBank: EXX64097.1), as well as the transcripts of the AMF-induced plant marker genes *RAM1*, *Vapyrin*, *STR1* and *PT4*. The signal abundance was

normalized to *NaIF-5a* (NCBI Reference Sequence: XP_019246749.1). The primer sequences are summarized in Table 4.

Transcript analysis of the apocarotenoid pathway

The transcript analysis of the (apo)carotenoid pathway was conducted based on RNA-seq (Data Set 3) by using *N. attenuata* roots with or without *R. irregularis* inoculations. The data analysis methods are based on the previously published pipeline of Ling *et al.* (2015). Representative values for transcripts abundances are TPM (Transcripts per kilobase of exon model per million mapped reads).

Blumenol transport experiment

To analyze the root-to-shoot transfer potential of blumenols, we placed three *N. attenuata* seedlings, previously germinated on petri dishes with GB5 Agar for approximately 10 days, into 0.5 mL reaction tubes. The roots were placed into the tube, while the shoot projected out of the tube. The tubes were carefully covered with parafilm, which held the seedlings in place and isolated roots from shoots (see Figure 6C). The tubes were filled with tap water supplemented with 0.5% v/v plant extracts enriched in Compounds 1 or 2 (unknown concentration; purified fractions), or a commercial available standard of Compound 6 (25 ng μL^{-1} end concentration; Roseoside; Wuhan ChemFaces Biochemical Co., Ltd.). Compound 1 or 2 were prepared from a mix of leaf tissues from different plant species (*M. truncatula, Z. mays, S. lypersicum* and *N. attenuata*) by methanol extraction followed by purification by SPE (Chromabond HR-XC column) and HPLC (Agilent-HPLC 1100 series; Phenomenex Luna C18(2), 250 × 10 mm, 5 µm; equipped with a Foxy Jr. fraction collector). As a control, we used tap water supplemented with the respective amounts of MeOH. The seedlings were incubated for 1d in a Percival climate chamber (16 h of light at 28 °C, and 8 h of dark at 26 °C). During sample collection, roots and shoots were separated and the roots were rinsed in water (to reduce the surface contamination with the incubation medium). While the shoots were analyzed separately, the roots of all seedlings from the same treatment were pooled. Sample extraction was conducted as described above.

Inducible PDS silencing

For the temporal and spatial restriction of PDS gene silencing, we treated the petiole of the second oldest stem leaf of AMF-inoculated and non AMF-inoculated i-ir*PDS* and EV plants with a 100 µM dexamethasone-containing lanolin paste (1% v/v DMSO). The lanolin paste was prepared and applied as described by Schäfer *et al.* (2013). The treatment started 3 weeks after potting and was conducted for 3 weeks. The lanolin paste was refreshed twice per week. On each plant the treated leaf and the adjacent, untreated leaves were harvested for analysis.

QTL analysis

The field experiments for QTL analysis were conducted in 2017. Collected leaf samples were extracted as described with 80% MeOH spiked with D_6-ABA as internal standard and analyzed with the method described under '*Method for targeted blumenol analysis in N. attenuata'*. The peak areas for Compound 2 were normalized by the amount of extracted tissue and internal standard and log-transformed. Samples with missing genotype or phenotype information were removed. In total, 728 samples were used for QTL mapping analysis. For quantitative trait loci (QTL) mapping, we used the AZ-UT RIL population and data analysis described by Zhou *et al.* (2017).

Statistics

Statistical analysis of the data was performed with R version 3.0.3 (http://www.R-project.org/). The statistical methods used and the number of replicates are indicated in the figure legends.

Acknowledgments

We thank the Brigham Young University for the use of their Lytle Preserve field station, Matthias Schöttner, Dechang Cao, Wenwu Zhou, Julia Cramer, Wibke Seibt and Eva Rothe for technical assistance, Danny Kessler, Andreas Schünzel, Andreas Weber, Jana Zitzmann from the glasshouse team for plant cultivation. This work was funded by the Max-Planck-Society, the ERC Advanced Grant (293926): ClockworkGreen and the Elsa Neumann Grant of Berlin, European Innovation Partnership Agri (276033540220041), Ministry of Consumer Protection, Food and Agriculture of the Federal Republic of Germany, Ministry for Science, Research and Culture of the State of Brandenburg, Thuringian Ministry of Infrastructure and Agriculture. Plant samples provided by the Harrison lab were generated with support from U.S. DOE # DE-SC0012460.

Competing interests

MW, MS, DL, RH, EM, SH, and ITB: European patent application EP 18 15 8922.7; ITB: Senior Editor, eLife

References

Adolfsson L, Nziengui H, Abreu IN, Šimura J, Beebo A, Herdean A, Aboalizadeh J, Široká J, Moritz T, Novák O, et al. 2017. Enhanced secondary- and hormone metabolism in leaves of arbuscular mycorrhizal *Medicago truncatula*. *Plant Physiology*.

Adolfsson L, Solymosi K, Andersson MX, Keresztes A, Uddling J, Schoefs B, Spetea C. 2015. Mycorrhiza symbiosis increases the surface for sunlight capture in *Medicago truncatula* for better photosynthetic production. *PLoS ONE* **10**(1): e0115314.

Aishan H, Baba M, Iwasaki N, Kuang H, Okuyama T. 2010. The constituents of *Urtica cannabina* used in Uighur medicine. *Pharmaceutical Biology* **48**(5): 577-583.

Aliferis KA, Chamoun R, Jabaji S. 2015. Metabolic responses of willow (*Salix purpurea* L.) leaves to mycorrhization as revealed by mass spectrometry and H-1 NMR spectroscopy metabolite profiling. *Frontiers in Plant Science* **6**: 15.

Baldwin IT. 1989. Mechanism of damage-induced alkaloid production in wild tobacco. *Journal of Chemical Ecology* **15**(5): 1661-1680.

Bhakuni DS, Joshi PP, Uprety H, Kapil RS. 1974. Roseoside-A C_{13} glycoside from *Vinca rosea*. *Phytochemistry* **13**(11): 2541-2543.

Bi HH, Song YY, Zeng RS. 2007. Biochemical and molecular responses of host plants to mycorrhizal infection and their roles in plant defence. *Allelopathy Journal* **20**(1): 15-27.

Borghi L, Kang J, Ko D, Lee Y, Martinoia E. 2015. The role of ABCG-type ABC transporters in phytohormone transport. *Biochemical Society Transactions* **43**: 924-930.

Bravo A, Brands M, Wewer V, Dormann P, Harrison MJ. 2017. Arbuscular mycorrhiza-specific enzymes FatM and RAM2 fine-tune lipid biosynthesis to promote development of arbuscular mycorrhiza. *New Phytologist* **214**(4): 1631-1645.

Brundrett M, Piche Y, Peterson R. 1985. A developmental study of the early stages in vesicular–arbuscular mycorrhiza formation. *Canadian Journal of Botany* **63**(2): 184-194.

Brundrett MC, Piché Y, Peterson RL. 1984. A new method for observing the morphology of vesicular–arbuscular mycorrhizae. *Canadian Journal of Botany* **62**(10): 2128-2134.

Brundrett MC, Tedersoo L. 2018. Evolutionary history of mycorrhizal symbioses and global host plant diversity. *New Phytologist*.

Bubner B, Gase K, Berger B, Link D, Baldwin IT. 2006. Occurrence of tetraploidy in *Nicotiana attenuata* plants after *Agrobacterium*-mediated transformation is genotype specific but independent of polysomaty of explant tissue. *Plant Cell Reports* **25**(7): 668-675.

Chitarra W, Pagliarani C, Maserti B, Lumini E, Siciliano I, Cascone P, Schubert A, Gambino G, Balestrini R, Guerrieri E. 2016. Insights on the impact of arbuscular mycorrhizal symbiosis on tomato tolerance to water stress. *Plant Physiology* **171**(2): 1009-1023.

Cutillo F, Dellagreca M, Previtera L, Zarrelli A. 2005. C_{13} norisoprenoids from *Brassica fruticulosa*. *Natural Product Research* **19**(2): 99-103.

De Kreij C, Voogt W, van den Bos AL, Baas R. 1997. *Voedingsoplossingen voor de teelt van tomaat in gesloten teeltsystemen*: Naaldwijk: Brochure VG Tomaat.

Fester T, Hause B, Schmidt D, Halfmann K, Schmidt J, Wray V, Hause G, Strack D. 2002. Occurrence and localization of apocarotenoids in arbuscular mycorrhizal plant roots. *Plant and Cell Physiology* **43**(3): 256-265.

Fester T, Maier W, Strack D. 1999. Accumulation of secondary compounds in barley and wheat roots in response to inoculation with an arbuscular mycorrhizal fungus and co-inoculation with rhizosphere bacteria. *Mycorrhiza* **8**(5): 241-246.

Fester T, Wray V, Nimtz M, Strack D. 2005. Is stimulation of carotenoid biosynthesis in arbuscular mycorrhizal roots a general phenomenon? *Phytochemistry* **66**(15): 1781-1786.

Floss DS, Levy JG, Levesque-Tremblay V, Pumplin N, Harrison MJ. 2013. DELLA proteins regulate arbuscule formation in arbuscular mycorrhizal symbiosis. *Proceedings of the National Academy of Sciences of the United States of America* **110**(51): E5025-5034.

Floss DS, Schliemann W, Schmidt J, Strack D, Walter MH. 2008. RNA interference-mediated repression of Mt*CCD1* in mycorrhizal roots of *Medicago truncatula* causes accumulation of C_{27} apocarotenoids, shedding light on the functional role of *CCD1*. *Plant Physiology* **148**(3): 1267-1282.

Foo E, Ross JJ, Jones WT, Reid JB. 2013. Plant hormones in arbuscular mycorrhizal symbioses: an emerging role for gibberellins. *Annals of Botany* **111**(5): 769-779.

Galbraith MN, Horn DHS. 1972. Structures of the natural products blumenols A, B, and C. *Journal of the Chemical Society, Chemical Communications*(3): 113-114.

Glawe GA, Zavala JA, Kessler A, Van Dam NM, Baldwin IT. 2003. Ecological costs and benefits correlated with trypsin protease inhibitor production in *Nicotiana attenuata*. *Ecology* **84**(1): 79-90.

Groten K, Nawaz A, Nguyen NHT, Santhanam R, Baldwin IT. 2015. Silencing a key gene of the common symbiosis pathway in *Nicotiana attenuata* specifically impairs arbuscular mycorrhizal infection without influencing the root-associated microbiome or plant growth. *Plant, Cell & Environment* **38**(11): 2398-2416.

Helber N, Wippel K, Sauer N, Schaarschmidt S, Hause B, Requena N. 2011. A versatile monosaccharide transporter that operates in the arbuscular mycorrhizal fungus *Glomus* sp is crucial for the symbiotic relationship with plants. *The Plant Cell* **23**(10): 3812-3823.

Hong JJ, Park YS, Bravo A, Bhattarai KK, Daniels DA, Harrison MJ. 2012. Diversity of morphology and function in arbuscular mycorrhizal symbioses in *Brachypodium distachyon*. *Planta* **236**(3): 851-865.

Hou X, Rivers J, León P, McQuinn RP, Pogson BJ. 2016. Synthesis and function of apocarotenoid signals in plants. *Trends in Plant Science* **21**(9): 792-803.

Jiang Y, Wang W, Xie Q, Liu N, Liu L. 2017. Plants transfer lipids to sustain colonization by mutualistic mycorrhizal and parasitic fungi. *Science* **356**(6343): 1172-1175.

Kato-Noguchi H, Hamada N, Clements DR. 2015. Phytotoxicities of the invasive species *Plantago major* and non-invasive species *Plantago asiatica*. *Acta Physiologiae Plantarum* **37**(3): 60.

Kato-Noguchi H, Tamura K, Sasaki H, Suenaga K. 2012. Identification of two phytotoxins, blumenol A and grasshopper ketone, in the allelopathic Japanese rice variety Awaakamai. *Journal of Plant Physiology* **169**(7): 682-685.

Keymer A, Pimprikar P, Wewer V, Huber C, Brands M. 2017. Lipid transfer from plants to arbuscular mycorrhiza fungi. *Elife* **6**: e29107.

Klingner A, Hundeshagen B, Kernebeck H, Bothe H. 1995. Localization of the yellow pigment formed in roots of gramineous plants colonized by arbuscular fungi. *Protoplasma* **185**(1-2): 50-57.

Krügel T, Lim M, Gase K, Halitschke R, Baldwin IT. 2002. *Agrobacterium*-mediated transformation of *Nicotiana attenuata*, a model ecological expression system. *Chemoecology* **12**(4): 177-183.

Lanfranco L, Fiorilli V, Venice F, Bonfante P. 2017. Strigolactones cross the kingdoms: plants, fungi, and bacteria in the arbuscular mycorrhizal symbiosis. *Journal of Experimental Botany*: erx432-erx432.

Lee G, Joo Y, Kim SG, Baldwin IT. 2017. What happens in the pith stays in the pith: tissue-localized defense responses facilitate chemical niche differentiation between two spatially separated herbivores. *The Plant Journal* **92**(3): 414-425.

Li D, Baldwin IT, Gaquerel E. 2015. Navigating natural variation in herbivory-induced secondary metabolism in coyote tobacco populations using MS/MS structural analysis. *Proceedings of the National Academy of Sciences of the United States of America* **112**(30): E4147-E4155.

Li D, Heiling S, Baldwin IT, Gaquerel E. 2016. Illuminating a plant's tissue-specific metabolic diversity using computational metabolomics and information theory. *Proceedings of the National Academy of Sciences of the United States of America* **113**(47): E7610-E7618.

Ling Z, Zhou W, Baldwin IT, Xu S. 2015. Insect herbivory elicits genome-wide alternative splicing responses in *Nicotiana attenuata*. *The Plant Journal* **84**(1): 228-243.

Liu J, Blaylock LA, Harrison MJ. 2004. cDNA arrays as a tool to identify mycorrhiza-regulated genes: identification of mycorrhiza-induced genes that encode or generate signaling molecules implicated in the control of root growth. *Canadian Journal of Botany* **82**(8): 1177-1185.

Luginbuehl LH, Menard GN. 2017. Fatty acids in arbuscular mycorrhizal fungi are synthesized by the host plant. *Science* **356**(6343): 1175-1178.

Maier W, Hammer K, Dammann U, Schulz B, Strack D. 1997. Accumulation of sesquiterpenoid cyclohexenone derivatives induced by an arbuscular mycorrhizal fungus in members of the *Poaceae*. *Planta* **202**(1): 36-42.

Maier W, Schmidt J, Nimtz M, Wray V, Strack D. 2000. Secondary products in mycorrhizal roots of tobacco and tomato. *Phytochemistry* **54**(5): 473-479.

Matsunami K, Otsuka H, Takeda Y. 2010. Structural Revisions of Blumenol C Glucoside and Byzantionoside B. *Chemical and Pharmaceutical Bulletin* **58**(3): 438-441.

Millner PD, Kitt DG. 1992. The Beltsville method for soilless production of vesicular-arbuscular mycorrhizal fungi. *Mycorrhiza* **2**(1): 9-15.

Nadal M, Sawers R, Naseem S, Bassin B, Kulicke C, Sharman A, An G, An K, Ahern KR, Romag A, et al. 2017. An *N*-acetylglucosamine transporter required for arbuscular mycorrhizal symbioses in rice and maize. *Nature plants* **3**: 17073-17073.

Paradi I, van Tuinen D, Morandi D, Ochatt S, Robert F, Jacas L, Dumas-Gaudot E. 2010. Transcription of two blue copper-binding protein isogenes is highly correlated with arbuscular mycorrhizal development in *Medicago truncatula*. *Molecular Plant-Microbe Interactions* **23**(9): 1175-1183.

Park H-J, Floss DS, Levesque-Tremblay V, Bravo A, Harrison MJ. 2015. Hyphal branching during arbuscule development requires *Reduced Arbuscular Mycorrhiza1*. *Plant Physiology* **169**(4): 2774-2788.

Peipp H, Maier W, Schmidt J, Wray V, Strack D. 1997. Arbuscular mycorrhizal fungus-induced changes in the accumulation of secondary compounds in barley roots. *Phytochemistry* **44**(4): 581-587.

Pineda A, Zheng SJ, van Loon JJ, Pieterse CM, Dicke M. 2010. Helping plants to deal with insects: the role of beneficial soil-borne microbes. *Trends in Plant Science* **15**(9): 507-514.

Ratcliff F, Martin-Hernandez AM, Baulcombe DC. 2001. Technical Advance. Tobacco rattle virus as a vector for analysis of gene function by silencing. *The Plant Journal* **25**(2): 237-245.

Rooney DC, Killham K, Bending GD, Baggs E, Weih M, Hodge A. 2009. Mycorrhizas and biomass crops: opportunities for future sustainable development. *Trends in Plant Science* **14**(10): 542-549.

Saedler R, Baldwin IT. 2004. Virus-induced gene silencing of jasmonate-induced direct defences, nicotine and trypsin proteinase-inhibitors in *Nicotiana attenuata*. *Journal of Experimental Botany* **55**(395): 151-157.

Schäfer M, Brütting C, Gase K, Reichelt M, Baldwin I, Meldau S. 2013. "Real time" genetic manipulation: A new tool for ecological field studies. *The Plant Journal* **76**: 506-518.

Schliemann W, Kolbe B, Schmidt J, Nimtz M, Wray V. 2008. Accumulation of apocarotenoids in mycorrhizal roots of leek (*Allium porrum*). *Phytochemistry* **69**(8): 1680-1688.

Schliemann W, Schmidt J, Nimtz M, Wray V, Fester T, Strack D. 2006. Accumulation of apocarotenoids in mycorrhizal roots of *Ornithogalum umbellatum*. *Phytochemistry* **67**(12): 1196-1205.

Schuman MC, Barthel K, Baldwin IT. 2012. Herbivory-induced volatiles function as defenses increasing fitness of the native plant *Nicotiana attenuata* in nature. *Elife* **1**: e00007.

Schweiger R, Baier MC, Persicke M, Müller C. 2014. High specificity in plant leaf metabolic responses to arbuscular mycorrhiza. *Nature Communications* **5**: 11.

Schweiger R, Müller C. 2015. Leaf metabolome in arbuscular mycorrhizal symbiosis. *Current Opinion in Plant Biology* **26**: 120-126.

Sharma E, Anand G, Kapoor R. 2017. Terpenoids in plant and arbuscular mycorrhiza-reinforced defence against herbivorous insects. *Annals of Botany* **119**(5): 791-801.

Strack D, Fester T. 2006. Isoprenoid metabolism and plastid reorganization in arbuscular mycorrhizal roots. *New Phytologist* **172**(1): 22-34.

Stuart KL, Coke LB. 1975. The effect of vomifoliol on stomatal aperture. *Planta* **122**(3): 307-310.

Takeda Y, Zhang H, Masuda T, Honda G, Otsuka H, Sezik E, Yesilada E, Handong S. 1997. Megastigmane glucosides from *Stachys byzantina*. *Phytochemistry* **44**(7): 1335-1337.

Toussaint JP. 2007. Investigating physiological changes in the aerial parts of AM plants: what do we know and where should we be heading? *Mycorrhiza* **17**(4): 349-353.

Vaccari DA, Strigul N. 2011. Extrapolating phosphorus production to estimate resource reserves. *Chemosphere* **84**(6): 792-797.

van de Wiel CCM, van der Linden CG, Scholten OE. 2016. Improving phosphorus use efficiency in agriculture: opportunities for breeding. *Euphytica* **207**(1): 1-22.

Vannette RL, Hunter MD, Rasmann S. 2013. Arbuscular mycorrhizal fungi alter above- and below-ground chemical defense expression differentially among *Asclepias* species. *Frontiers in Plant Science* **4**: 361.

Vierheilig H, Schweiger P, Brundrett M. 2005. An overview of methods for the detection and observation of arbuscular mycorrhizal fungi in roots. *Physiologia Plantarum* **125**(4): 393-404.

Vogel JT, Walter MH, Giavalisco P, Lytovchenko A, Kohlen W, Charnikhova T, Simkin AJ, Goulet C, Strack D, Bouwmeester HJ, et al. 2010. Sl*CCD7* controls strigolactone biosynthesis, shoot branching and mycorrhiza-induced apocarotenoid formation in tomato. *The Plant Journal* **61**(2): 300-311.

Zhou W, Kugler A, McGale E, Haverkamp A, Knaden M, Guo H, Beran F, Yon F, Li R, Lackus N, et al. 2017. Tissue-specific emission of (E)-alpha-bergamotene helps resolve the dilemma when pollinators are also herbivores. *Current Biology* **27**(9): 1336-1341.

Figure legends

Figure 1 Blumenol core structures and exemplary modifications

A Structure of blumenol A, blumenol B and blumenol C. **B** Exemplary blumenol C derivatives. Glyc, glycoside.

Figure 2 Combined targeted and untargeted metabolomics identified blumenol derivatives as AMF-indicative *in-planta* metabolic fingerprints in the roots and leaves of *Nicotiana attenuata* plants.

A Experimental set-up. EV and ir*CCaMK* plants were co-cultured and inoculated with or without *R. irregularis*. Six weeks after inoculation (wpi), root samples were harvested for metabolite profiling. **B** Covariance network visualizing *m/z* features from UHPLC-qTOF-MS untargeted analysis (n=8). Known compounds, including nicotine, phenylalanine and various phenolics, and unknown metabolites (Unk.) are enclosed in dashed ellipses. **C** Normalized Z-scored of *m/z* features were clustered using STEM Clustering; 5 of 8 significant clusters are shown in different colors and mapped onto the covariance network. The intensity variation (mean + SE) of 2 selected features (Compounds 1 and 2) are shown in bar plots (n.d., not detected). **D** Representative chromatograms of Compounds 1 and 2 in roots and leaves of plants with and without AMF inoculation, as analyzed by targeted UHPLC-triple quadrupole-MS metabolomics.

Figure 2—figure supplement 1 Abundance of root blumenol derivatives correlates positively with root AMF colonization.

A Time lapse accumulations (3-7 weeks post inoculation, n≥3 for each time point) of Compounds 1, 2, 3, 4 and 5 in roots of plants with (EV+, black lines with circles) and without (EV-, grey lines with triangle) AMF inoculation. The experiment was conducted with empty vector (EV) transformed plants. Data are means ± SE. **B** Abundance of Compounds 1, 2, 3, 4 and 5 relative to the transcript abundance of the *R. irregularis* specific housekeeping gene, *Ri-tub* (GenBank: EXX64097.1), as well as to the plant-derived marker genes *RAM1*, *Vapyrin*, *STR1* and *PT4* (Gene ID and transcripts abundance are listed in Data Set 1). The transcript abundance was quantified by q-PCR, relative to *NaIF-5a* (NCBI Reference Sequence: XP_019246749.1). The correlations among blumenol derivatives and the transcript abundances of marker genes were analyzed by linear regression (lm) models.

Figure 3 Compounds 1 and 2 are leaf markers of root AMF colonization in *N. attenuata*.

A Time lapse accumulations of Compounds 1 and 2 in leaves of EV plants with (EV+, red) or without (EV-, black) AMF-inoculation and of ir*CCaMK* plants with AMF-inoculation (ir*CCaMK*+, orange, covered by black) (means ± SE, n≥5). **B** Leaf abundances of Compounds 1 and 2 (5 wpi) of plants inoculated with different inoculum concentrations (means + SE, n≥4); different letters indicate significant differences ($p < 0.05$, one-way ANOVA followed by Fisher's LSD). **C** Compounds 1 and 2 in leaf samples of EV and ir*CCaMK* plants inoculated with (+) or without (-) AMF inoculum isolated from the plant's native habitat (6 wpi); different letters indicate significant differences ($p < 0.05$, one-way ANOVA followed by Tukey's HSD, n=10). **D** Field experiment (Great Basin Desert, Utah, USA): Compounds 1 and 2 in leaf samples of EV (n=20) and ir*CCaMK* (n=19) plants sampled 8 weeks after planting. (Student's *t*-test: ***, p<0.001). **E** Representative images of WGA-488 stained roots of plants shown in **B** (bar=100 µm). **F** Leaf Compounds 1 and 2 relative to the percentage of root colonization by hyphae, arbuscules, vesicles and total root length colonization of the same plants (linear regression model). **G** Compounds 1 and 2 in 17 different tissues of plants with (+AMF, n=3, red bars) or without (-AMF, n=1, black bars) AMF-inoculation harvested at 6 wpi.

Figure 3—figure supplement 1 AMF-induced accumulation of blumenol derivatives in roots and leaves of *N. attenuata*.

A Representative chromatograms of targeted tandem MS-based analyses of Compounds 3, 4 and 5 in roots (bottom panel) and leaves (top panel) of *N. attenuata* plants after inoculation with *R. irregularis* (+*R. irregularis*, red line, 6wpi) and in untreated control plants (Control, black line). Experiments were conducted with wild type (WT) plants. The respective precursor-to-product ion transitions are indicated at the top. **B**, **D** Representative chromatograms of a high resolution MS-based analysis of Compounds 1, 3, 4 and 5 (**B)**, as well as Compound 2 (**D)** in roots (bottom panel) and leaves (top panel) of *N. attenuata* plants after inoculation with *R. irregularis*. Extracted ion chromatograms (EIC) are labeled by colors and settings listed at the top. **C**, **E** Comparison of fragmentation patterns of Compounds 1 (**C**) and 2 (**E**) in both tissues by high resolution tandem MS.

Figure 3—figure supplement 2 Time course analysis of the root colonization by AMF and the corresponding accumulation of Compounds 1 and 2 in roots and leaves of *N. attenuata*.

A Root colonization in EV plants at different time points after inoculation with *R. irregularis* (2/3/4/5 wpi). H: hyphae; A: arbuscules; V: vesicles; Total: total root length colonization (means + SE; n=8). **B, C** Abundances of Compounds 1 and 2 in roots (**B**) and leaves (**C**) of plants at

different time points after inoculation with *R. irregularis* (2/3/4/5 wpi; means + SE; n≥5). Different letters indicate significant differences ($p < 0.05$, one-way ANOVA followed by Tukey's HSD). n.d., not detected.

Figure 3—figure supplement 3 Root AMF colonization and abundance of Compound 1 in a second independently transformed ir*CCaMK* line.

A Root colonization analysis in EV and ir*CCaMK* (A-09-1208-6) plants. H: hyphae; A: arbuscules; V: vesicles; Total: total root length colonization (means + SE; EV, n=9; ir*CCaMK;* n=7). **B** Transcript abundance of AMF marker genes in roots of EV and ir*CCaMK* plants inoculated with *R. irregularis* (6 wpi; means + SE; n=6). **C** Compound 1 levels in roots and leaves of EV and ir*CCaMK* plants inoculated with *R. irregularis* (6 wpi; means + SE; n=8).

Figure 3—figure supplement 4 Signals from Compound 1 are partially disturbed in field samples, but not for Compound 2.

Leaf samples were harvested from glasshouse-(top panel) and field-grown, Utah, 2016 (bottom panel) plants for analysis. Representative chromatograms of two samples of each genotype, EV (red) and ir*CCaMK* (black), were shown. Grey area indicates the peak integration window used for the quantification of Compound 1.

Figure 4 Transcript abundance of classical arbuscular mycorrhizal symbiosis-marker genes do not respond in leaves of mycorrhizal and control *N. attenuata* plants

The transcript abundance (relative to *NaIF-5a*) of classical root marker genes was analyzed in leaves of *N. attenuata* plants in the presence (+*R. irregularis*, black bars) and absence (control, white bars) of root colonization with *R. irregularis.* The marker genes include the *R. irregularis* specific housekeeping gene, *Ri-tub*, as well as the plant-derived marker genes *CCaMK*, *Vapyrin*, *PT4*, *STR1* and *RAM1*. Leaf samples were harvested 6 weeks after inoculation and analyzed by qPCR. Data represent means + SE (n≥3), n.d., not detected.

Figure 5 Different biotic and abiotic stresses do not elicit accumulations of Compounds 1 and 2 in leaves.

A-D Representative leaves of *N. attenuata* plants subjected to different stresses (right leaf), as well as the untreated controls (left leaf): **A** *Manduca sexta* feeding for 10 days; **B** *Botrytis cinerea* infection for 5 days. **C** Infection for 2 weeks with *Agrobacterium tumefaciens* carrying the Tobacco Rattle Virus; **D** Dehydration for 3 days. For each treatment, four biological replicates were used. **E** Accumulation of Compounds 1 and 2 in treated samples from **A-D**. n.d., not detected.

Figure 6 AMF-indicative Compounds 1 and 2 in shoots of mycorrhizal plants originate from the roots.

A Hierarchical clustering analysis of transcript abundance from RNA-seq of methylerythritol 4-phosphate (MEP) and (apo)carotenoid biosynthetic genes (for details see Figure S6A). **B** Compounds 1, 2 (AMF-specific) and 6 (not AMF-specific) in AMF-inoculated i-irPDS and EV plants. On each plant, a single stem leaf (leaf 0) was elicited with 100 μM DEX-containing paste for 3 weeks; treated and adjacent, untreated control leaves (leaf -1 and leaf+1) were harvested. Representative leaves are shown (bleaching indicates PDS silencing); (means + SE, n≥6). The same leaf positions in i-irPDS and EV plants were compared by Student's *t*-tests. **C** Contents of Compounds 1, 2 and 6 in the roots and shoots of seedlings whose roots were dipped for 1 d into an aqueous solution with (treatment) or without (control) AMF-indicative blumenols. **D** Model of blumenol distribution in plants with (right panel) and without (left panel) AMF colonization. The model illustrates constitutive blumenols (e.g., Compound 6 in *N. attenuata*) and AMF-indicative ones (e.g., Compounds 1 and 2 in *N. attenuata*) and their inferred transport.

Figure 6—figure supplement 1 Foliar levels of Compounds 1 and 2 are derived from roots

A Transcript abundance of MEP and apocarotenoid pathway biosynthetic genes (based on homologies to tomato, Arabidopsis and tobacco). Plant materials from same experimental set-up as in Figure1A were used for sequencing. Data are means + SE (n=3) generated by RNA-seq and the abundance of each transcript is expressed in TPM (Transcripts per kilobase of exon model per million mapped reads). Transcripts were analyzed in roots (left panel, orange background) and leaf tissues (right panel, green background) of EV and ir*CCaMK* plants with (EV+ and ir*CCaMK*+ respectively) and without (EV- and ir*CCaMK*- respectively) inoculations with *R. irregularis.* Gene abbreviations; CRTISO: carotenoid isomerase; GGPPs: geranylgeranyl diphosphate synthase; PSY: phytoene synthase; PDS: phytoene desaturase; ZDS: ζ-carotene de-saturase; Z-ISO: ζ- carotene isomerase; CCD: carotenoid cleavage dioxygenase; MAX1: cytochrome P450-type monooxygenase CYP711A1; DXS: 1-deoxy-D-xylulose 5-phosphate synthase; DXR: 1-deoxy-D-xylulose 5-phosphate reductoisomerase; MCT: 2-C-methyl-D-

erythritol 4-phosphate cytidylyltransferase; CMK: 4-(cytidine 5′-diphospho)-2-C-methyl-D-erythritol kinase; MDS: 2-C-methyl-D-erythritol 2,4-cyclodiphosphate synthase; HDS: 4-hydroxy-3-methylbut-2-enyl-diphosphate synthase; HDR: 4-hydroxy-3-methylbut-2-enyl diphosphate reductase; D27: carotenoid isomerase. **B** Representative chromatograms from a targeted tandem MS-based analysis of Compounds 1, 2 and 6 in stem sap fluid of *N. attenuata* plants after *R. irregularis* inoculation (+AMF, red line, 6wpi) and of untreated control plants (Control, black line). The respective precursor-to-product ion transitions are indicated at top. **C** Accumulations of Compounds 1, 2 and 6 in non AMF-inoculated plants after local silencing of the carotenoid biosynthesis in the DEX-treated leaf. The experiment was performed with plants harboring a transformation construct mediating the chemically-inducible silencing of the phytoene desaturase (i-irPDS), as well as with empty vector (EV) plants. On each plant, a single stem leaf (leaf 0) was treated with a 100 μM dexamethasone (DEX) containing lanolin paste for 3 weeks. The adjacent, untreated leaves (leaf -1 and leaf+1) were harvested as controls. Representative leaves are shown (bleaching indicates functional PDS silencing). Data are means + SE (n≥6). For statistical analysis, the samples from the same leaf positions in i-irPDS and EV plants were compared by Student's *t* test. **D** Contents of Compounds 1, 2 and 6 in the roots (red bars) and shoots (blue bars) of seedlings whose roots were dipped into an aqueous solution with or without addition of the respective blumenols. Seedlings were incubated for 1d before analysis. Data are means + SE (shoot, n=3; root, n=1). The data originate from the same experiment presented in Figure 6C.

Figure 6—figure supplement 2 Compound 6 is constitutively produced in shoots of *N. attenuata* and not indicative of AMF associations.

A Representative chromatograms from a targeted tandem MS-based analysis of Compound 6 in leaves of *N. attenuata* (bottom panel) and as comparison, a blumenol A-9-O-glucoside (roseoside) standard (top panel). The precursor-to-product ion transitions are indicated. **B** Time lapse accumulations of Compound 6 in roots of EV plants with (EV+, green line) or without (EV-, black line) AMF-inoculation. Data represent means ± SE (n≥3). **C** Time lapse accumulations of Compound 6 in leaves of EV plants with (EV+, red line) or without (EV-, black line) AMF-inoculation and of ir*CCaMK* plants with AMF-inoculation (ir*CCaMK*+, orange line). Data represent means ± SE (n≥5). **D** Comparison of the abundances of Compound 6 in leaves of plants inoculated with different inoculum concentrations, samples were harvested at 5 weeks-post-inoculation (wpi). Data are means + SE (n≥4). Different letters indicate significant differences ($p < 0.05$, one-way ANOVA followed by Fisher's LSD). **E** Field experiment (Great Basin Desert, Utah, USA): leaf samples of EV (n=20) and ir*CCaMK* (n=19) plants were sampled 8 weeks after planting and amounts of Compound 6 were analyzed. For statistical analysis, Student's *t* test was applied. **F** Abundance of Compound 6 relative to the transcript abundance of the *R. irregularis* specific housekeeping gene, *Ri-tub* (GenBank: EXX64097.1), as well as to the

plant derived marker genes *RAM1, Vapyrin, STR1* and *PT4*.The transcript abundance was quantified by q-PCR, relative to *NaIF-5a* (NCBI Reference Sequence: XP_019246749.1). The correlation between compound 6 and transcript abundance of marker genes was analyzed by linear regression (lm) models. **G** Distribution of Compound 6 in different plant tissues, as indicated, of plants with (+AMF, n=3, red bars) or without (-AMF, n=1, black bars) AMF-inoculation. Samples were harvested at 6 wpi.

Figure 7 AMF-indicative changes in blumenols in aerial plant parts are valuable research tools providing accurate assessments of functional AMF associations in high-throughput screenings of multiple plant and AMF species.

A Root colonization analysis in two *N. attenuata* accessions (UT/ AZ). H: hyphae; A: arbuscules; V: vesicles; Total: total root length colonization (n=4; Student's *t*-test, *, $p<0.05$, **, $p<0.01$, ***, $p<0.001$). **B** Representative images of trypan blue stained roots (6 wpi; bar=100 μm). **C** Compound 2 in roots and leaves of UT and AZ plants with and without AMF-inoculation (means + SE, n=8). **D** Heatmap of the normalized abundance of foliar Compound 2 in plants of a UT-AZ RIL population (728 plants) planted across a 7,200 m^2 field plot. **E** QTL mapping analysis of the data from **D.** QTL locus on linkage group 3 contains Na*NOPE1*, an AMF-associated gene, in addition to others. LOD, logarithm of the odds ratio. **F** Blumenol contents of different crop and model plants with and without AMF inoculation (*S. lycopersicum* (n=6), *T. aestivum* (n=10), *H. vulgare* (n=5): 8 wpi; *M. truncatula* (n=3): 7 wpi; *S. tuberosum* (n=5): 6 wpi; *B. distachyon* (n=4): 5 wpi). Different plant and AMF species were used as indicated (means + SE; n.d., not detected).

Figure 7—figure supplement 1 Phenotypes of UT and AZ accessions and field plot planting design.

A Representative *N. attenuata* plants of the UT and AZ accessions in the rosette stages of growth (12 days after potting). **B** Transcripts of marker genes in roots responding to AMF colonization in UT and AZ after 6 wpi inoculated with *R. irregularis* were quantified by qPCR in the same samples as in Fig 4A-C (n=8); Student's *t* test *, $p<0.05$, **, $p<0.01$, ***, $p<0.001$. **C** Field plot of 728 sampled individual plants in Utah, USA, 2017.

Figure 7—figure supplement 2 AMF-indicative changes in blumenols in aerial plant part are valuable research tools providing accurate assessments of functional AMF associations of multiple plant and AMF species (continued from Figure 7F).

Blumenol contents of different crop plants with and without AMF inoculation (*T. aestivum*: 8 wpi, n=5; *H. vulgare*: 8 wpi, n=10; *S. lycopersicum* with *F. mossae*: 6wpi, n=5; *S. lycopersicum* with *R. irregularis*: 11wpi, n=6; *B. distachyon*: 5 wpi, n=4; *M. truncatula*: 7 wpi, n=3). Different plant and AMF species were used, as indicated; means + SE, n.d., not detected.

Table 1 ^{1}H and ^{13}C NMR data for compounds 1-4 and 7

No.	Compound 1			Compound 2			Compound 3			Compound 4			Compound 7		
Pos.	δ_H	mult., J [Hz]	δ_C	δ_H	mult., J [Hz]	δ_C	δ_H	mult., J [Hz]	δ_C	δ_H	mult., J [Hz]	δ_C	δ_H	mult., J [Hz]	δ_C
1	-	-	202.3	-	-	203.1	-	-	202.2	-	-	202.3	-	-	200.9
2	6.06	dd, 1.8/1.8	121.3	6.40	s	128.5	6.06	s br	121.3	5.81	s br	125.2	5.82	s	126.4
3	-	-	172.4	-	-	172.6	-	-	172.2	-	-	169.8	-	-	171.5
4	1.92	dd, 5.2/5.2	47.8	2.64	m	46.3	1.92	dd, 5.2/5.2	48.0	1.97	dd, 5.0/5.0	52.4	-	-	79.2
5	-	-	37.2	-	-	36.9	-	-	37.2	-	-	37.2	-	-	42.9
6	2.59 2.02	d, 17.5 d, 17.5	48.5	2.03 2.60	d, 17.4 d, 17.4	48.0	2.59 2.02	d, 17.6 d, 17.6	47.7	2.49 1.98	d, 17.3 d, 17.3	48.0	2.13 2.16	d, 18.0 d, 18.0	50.8
7	1.66 1.82	m m	26.8	1.62 1.88	m m	27.6	1.66 1.82	m m	27.1	1.69 1.80	m m	26.5	1.83 2.07	m m	34.6
8	1.63	m	37.1	1.60	m	36.0	1.63	m	37.2	1.68 1.61	m m	37.4	1.49 1.78	m m	32.7
9	3.82	dd, 6.2/11.7	77.2	3.80	m	77.7	3.83	dd, 6.3/11.7	77.7	3.83	dd, 6.3/11.6	77.7	3.80	ddd, 6.3/11.8/11.8	78.2
10	1.24	d, 6.2	21.6	1.21	d, 6.1	21.9	1.24	d, 6.3	21.9	1.25	d, 6.3	21.9	1.24	d, 6.3	21.9
11	4.32 4.16	dd, 17.8/1.8 dd, 17.8/1.8	64.9	-	-	160.1	4.33 4.16	m/m	64.9	2.05	d, 1.2	24.9	2.04	d, 1.0	21.7
12	1.02	s	28.4	1.01	s	28.4	1.02	s	28.6	1.02	s	28.7	1.01	s	24.3
13	1.12	s	27.5	1.12	s	27.5	1.11	s	27.5	1.10	s	27.4	1.09	s	23.7
1'	4.31	d, 7.9	103.8	4.30	d, 7.9	104.1	4.32	d, 7.9	103.8	4.32	d, 7.8	104.0	4.31	d, 7.9	104.0
2'	3.15	dd, 7.9/9.0	75.0	3.13	dd, 7.9/8.9	75.1	3.15	dd, 7.9/9.0	75.1	3.16	dd, 7.8/9.0	75.2	3.14	dd, 7.9/8.9	75.1
3'	3.33	dd, 9.0/9.0	77.9	3.35	dd, 8.9/8.9	78.0	3.33	m	77.8	3.34	dd, 9.0/9.0	78.0	3.33	dd, 8.9/8.9	77.8
4'	3.27	dd, 9.0/9.0	71.4	3.27	dd, 8.9/8.9	71.5	3.33	m	71.4	3.33	dd, 9.0/9.0	71.5	3.27	dd, 8.9/8.9	71.4
5'	3.25	m	77.6	3.25	m	77.6	3.45	m	77.0	3.44	m	76.9	3.24	m	77.7
6'	3.85 3.65	dd, 11.8/2.2 dd, 11.8/5.5	62.5	3.84 3.66	dd, 2.0/12.3 dd, 5.0/12.3	62.6	4.11 3.78	dd, 11.7/2.0 dd, 11.7/5.7	69.6	4.11 3.79	dd, 11.6/1.6 dd, 11.6/5.9	69.7	3.85 3.65	d, 11.7 dd, 4.5/11.7	62.3
1"							4.40	d, 7.9	104.6	4.40	d, 7.8	104.8			
2"							3.21	dd, 7.9/9.0	74.9	3.21	dd, 7.8/9.0	75.0			
3"							3.34	dd, 9.0/9.0	77.9	3.34	dd, 9.0/9.0	77.9			
4"							3.28	dd, 9.0/9.0	71.4	3.28	dd, 9.0/9.0	71.5			
5"							3.26	m	77.9	3.26	ddd, 9.0/5.4/1.8	78.0			
6"							3.87 3.66	dd, 11.9/2.0 dd, 11.9/5.2	62.5	3.86 3.66	dd, 11.6/1.8 dd, 11.6/5.4	62.7			

s, singlet; s br, broad singlet; d, doublet; dd, doublet of doublet; m, multiplet

Table 2 MRM-settings used for targeted blumenol analysis

Nr.	Compound Name	RT	Q1 [m/z] [a, b]			Q3 [m/z] [c, d] (CE [V])
1	11-hydroxyblumenol C-Glc [f, g]	2.82	+	389.22	227.16 (-2.5), **209.15 (-7.5)**, 191.14 (-12.5), 163.10 (-15), 149.10 (-17.5)
2	11-carboxyblumenol C-Glc [f, g]	3.22	+	403.22	241.16 (-2.5), 223.15 (-7.5), 177.10 (-15), 195.14 (-12.5)
			+	241.16 [e]	223.15 (-5), 177.10 (-15), **195.14 (-10)**
3	11-hydroxyblumenol C-Glc-Glc [f, g]	2.5	+	551.27	389.22 (-2.5), 227.16 (-7.5), **209.15 (-10)**, 191.14 (-15), 149.10 (-20)
4	Blumenol C – Glc-Glc [f, g]	3.47	+	535.27	373.22 (-2.5), **211.00 (-10)**, 193.10 (-17.5), 135.00 (-22.5), 109.00 (-22.5)
5	Blumenol C - Glc [f, h]	4.18	+	373.22	**211.20 (-6)**, 193.16 (-9), 175.10 (-15), 135.12 (-16), 109.10 (-20)
6	Blumenol A - Glc [f, h]	2.51	-	385.20	**153.10 (14)**
			+	387.20	225.15 (-5), 207.14 (-8), 149.10 (-18), 135.12 (-16), 123.08 (-23)
7	Blumenol B - Glc [f, g]	2.5	+	389.22	227.16 (-5), **209.15 (-7.5)**, 191.14 (-12.5), 153.10 (-17.5), 149.10 (-17.5)
8	Blumenol C – Glc-GlcU [f, i]	3.25 & 3.38	+	549.27	373.22 (-2.5), **211.00 (-10)**, 193.10 (-17.5), 135.00 (-22.5), 109.00 (-22.5)
9	11-hydroxylumenol C – Glc-Rha [i]	2.8	+	535.27	389.22 (-2.5), **227.16 (-7.5)**, 209.15 (-10), 191.14 (-15), 149.10 (-20)
10	Blumenol C – Glc-Rha [f, i]	4.1	+	519.27	373.22 (-2.5), **211.00 (-10)**, 193.10 (-17.5), 135.00 (-22.5), 109.00 (-22.5)
11	Hydroxyblumenol C-Hex-Pen [i]	2.5	+	521.27	389.22 (-2.5), 227.16 (-7.5), **209.15 (-10)**, 191.14 (-15), 149.10 (-20)
	D_6-ABA [h]	4.5	-	269.17	**159.00 (10)**

RT: retention time
CE: collision energy
Glc: glucose
GlcU: glucuronic acid
Rha: rhamnose
Hex: hexose
Pen: pentose
[a] Resolution: 0.7
[b] $[M+H]^+$ or $[M-H]^-$ if not stated differently
[c] Resolution: 2
[d] Quantifiers are depicted in bold
[e] $[M+H-Glc]^+$
[f] Verified by high resolution MS
[g] Verified by NMR
[h] Optimized with commercial available standards
[i] Transitions predicted based on structural similar compounds and literature information

Table 3 MRM-settings for the analysis of selected blumenols in *N. attenuata*

Nr.	Compound Name	RT	Q1 [m/z] [a, b]			Q3 [m/z] [c, d] (CE [V])
1	11-hydroxyblumenol C-Glc [f, g]	2.82	+	389.22		227.16 (-2.5), **209.15 (-7.5)**, 191.14 (-12.5), 163.10 (-15), 149.10 (-17.5)
2	11-carboxyblumenol C-Glc [f, g]	3.22	+	403.22		241.16 (-2.5), 223.15 (-7.5), 177.10 (-15), 195.14 (-12.5)
			+	241.16 [e]		223.15 (-5), 177.10 (-15), **195.14 (-10)**
6	Blumenol A - Glc [f, h]	2.51	-	385.20		**153.10 (14)**
			+	387.20		225.15 (-5), 207.14 (-8), 149.10 (-18), 135.12 (-16), 123.08 (-23)
	D_6-ABA [h]	4.0	-	269.17		**159.00 (10)**

RT: retention time
CE: collision energy
Glc: glucose
Hex: hexose
Pen: pentose
[a] Resolution: 0.7
[b] $[M+H]^+$ or $[M-H]^-$ if not stated differently
[c] Resolution: 2
[d] Quantifiers are depicted in bold
[e] $[M+H-Glc]^+$
[f] Verified by high resolution MS
[g] Verified by NMR
[h] Optimized with commercial available standards

Table 4 Sequences of primers used for qPCR-based analysis of AMF-colonization rates

Gene	Forward primer	Reversed primer
NaIF-5a	GTCGGACGAAGAACACCATT	CACATCACAGTTGTGGGAGG
NaRAM1	ACGGGGTCTATCGCTCCTT	GTGCACCAGTTGTAAGCCAC
NaVapyrin	GGTCCCAAGTGATTGGTTCAC	GACCTTCAAAGTCAACTGAGTCAA
NaSTR1	TCAGGCTTCCACCTTCAATATCT	GACTCTCCGACGTTCTCCC
NaPT4	GGGGCTCGTTTCAATGATTA	AACACGATCCGCCAAACAT
NaCCaMK	TTGGAGCTTTGTTCTGGTGGT	ATACTTGCCCCGTGTAGCG
NaNOPE1	ACTTGATGCCATGTTTCAGAGC	TCCAATTCGCGATAAGCTGGT
Ri-TUB	TGTCCAACCGGTTTTAAAGT	AAAGCACGTTTGGCGTACAT

Source data files

Figure 2-source data
Figure 2-figure supplement 1-source data

Figure 3-source data
Figure 3-figure supplement 2-source data
Figure 3-figure supplement 3-source data

Figure 4-source data

Figure 6-source data
Figure 6-figure supplement 1-source data
Figure 6-figure supplement 2-source data

Figure 7-source data
Figure 7-figure supplement 1-source data
Figure 7-figure supplement 2-source data

Source Code File for QTL analysis

A

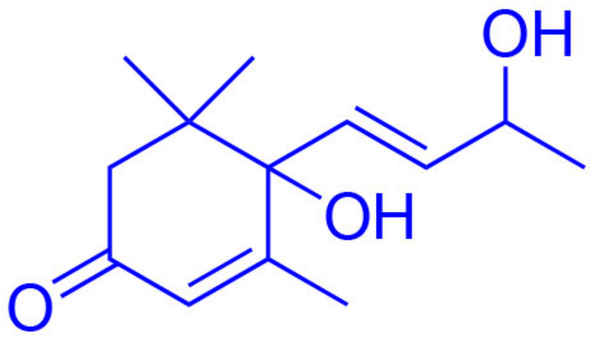

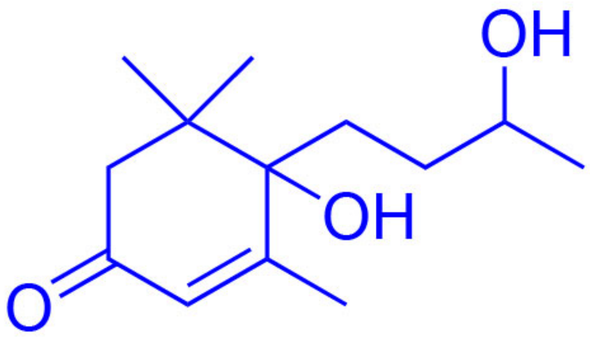

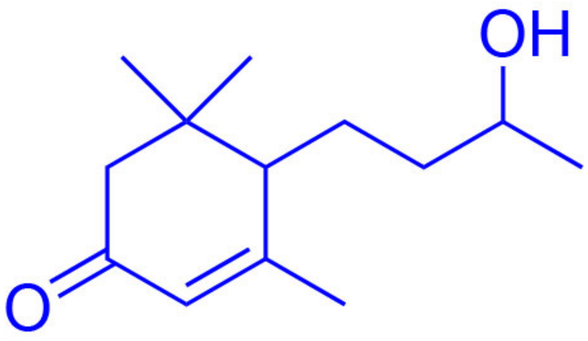

B

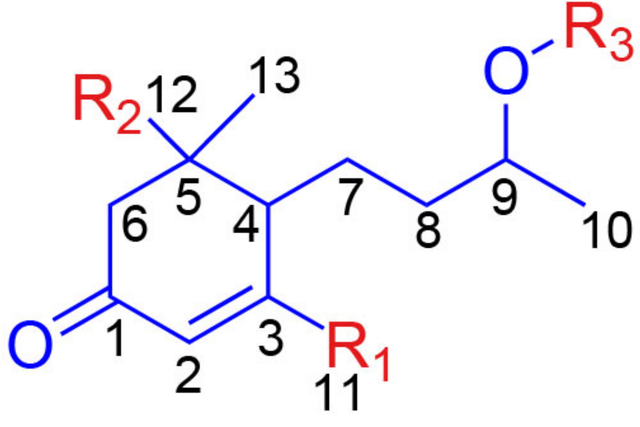

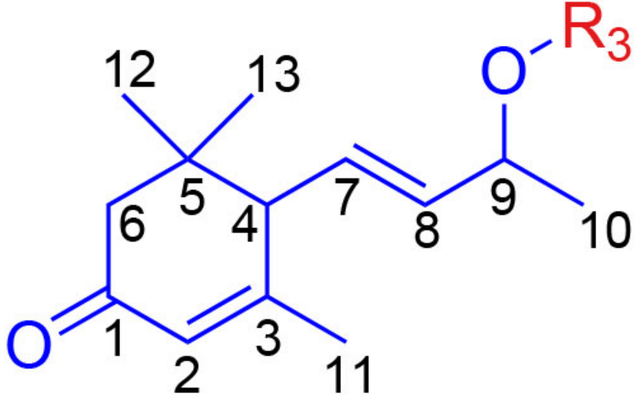

R_1	R_2	R_3
$-CH_3$	$-CH_3$	-H
$-CH_2OH$	-COOH	-Glyc
-COOH		

A

EV-
irCCaMK-
EV+
irCCaMK+
Control
+R. irregularis
Root

B

Root metabolome profiling
Untargeted analysis

m/z features
PCC>0.8

Unk.
Unk.
Unk.
Unk.
Phenolics
Nicotine
Phenylalanine

C

STEM Pattern Recognition
Structure elucidation
Intensity (Z-score)
STEM clusters

Relative abundance in roots [peak area g FM^{-1}]

x10^4
m/z 389.22
@ 475s
[M+H]$^+$
n.d
n.d
Glc
OH
[C$_{19}$H$_{32}$O$_8$+H]$^+$
1

x10^3
m/z 403.19
@ 535s
[M+H]$^+$
n.d
n.d
Glc
COOH
[C$_{19}$H$_{30}$O$_9$+H]$^+$
2

EV-
irCCaMK-
EV+
irCCaMK+

D

Root-shoot comparison
Targeted analysis

WT
Leaf
Root

1
389.2>209.1
2
241.2>195.1
Signal intensity [kcps]
RT [min]
Control
+ R. irregularis

Injection Volume:
Leaf: 5 µL
Root: 2 µL

A

B

1

2

3

4

5

Glc

GlcGlc

OH

COOH

EV (+AMF)

EV (-)

Relative abundance [peak area g FM^{-1}]

Weeks post inoculation

Transcript abundance (relative to *IF−5a*)

Ri-TUB

RAM1

Vapyrin

STR1

PT4

r^2=0.891 p< 2.2e-16

r^2=0.893 p< 2.2e-16

r^2=0.888 p< 2.2e-16

r^2=0.699 p=1.913e-11

r^2=0.786 p=2.775e-14

r^2=0.849 p< 2.2e-16

r^2=0.864 p< 2.2e-16

r^2=0.841 p< 2.2e-16

r^2=0.731 p=2.119e-12

r^2=0.714 p=7.217e-12

r^2=0.597 p=5.1e-09

r^2=0.486 p=5.8e-07

r^2=0.497 p=3.8e-07

r^2=0.356 p=4.9e-05

r^2=0.283 p=4.1e-04

r^2=0.917 p< 2.2e-16

r^2=0.806 p=4.28e-15

r^2=0.801 p=6.43e-15

r^2=0.593 p=6.37e-09

r^2=0.659 p=2.06e-10

r^2=0.807 p=3.9e-15

r^2=0.779 p=4.9e-14

r^2=0.808 p=3.4e-15

r^2=0.622 p=1.5e-09

r^2=0.618 p=1.9e-09

x100

A

B

C

D

Relative abundance [peak area g FM^{-1}]

irCCaMK (+)
EV (+)
EV (-)
irCCaMK (-)

x10^6
x10^5

n.d
a
b
bc
c

***

Compound ①
Compound ②
Glc
OH
COOH

Weeks post inoculation
Inoculum gradient
Native inoculum
(Glasshouse experiment)
Field 2016
irCCaMK EV

E

Inoculum gradient

1:60
1:40
1:20
1:10
1
100 µm

F

Relative abundance [peak area g FM^{-1}]

Hyphae
Arbuscule
Vesicle
Total

r^2=0.0033, p=0.76
r^2=0.699, p=8.461e-09
r^2=0.658, p=5.457e-08
r^2=0.746, p=7.944e-10
r^2=0.0072, p=0.65
r^2=0.607, p=2.448e-07
r^2=0.4136, p=9.544e-05
r^2=0.589, p=4.671e-07

Percentage of root colonization [%]

G

+AMF
-AMF

C: Capsule
F: Flower
FB: Flower bud
ST: Stem
S: Stem leaf
R: Rosette leaf

C
F
FB
ST
S7
S6
S5
S4
S3
S2
S1
R1
R2
R3
R4
R5
Root

x100
x10

Relative abundance
[ng g FM^{-1}, ABA equivalents]

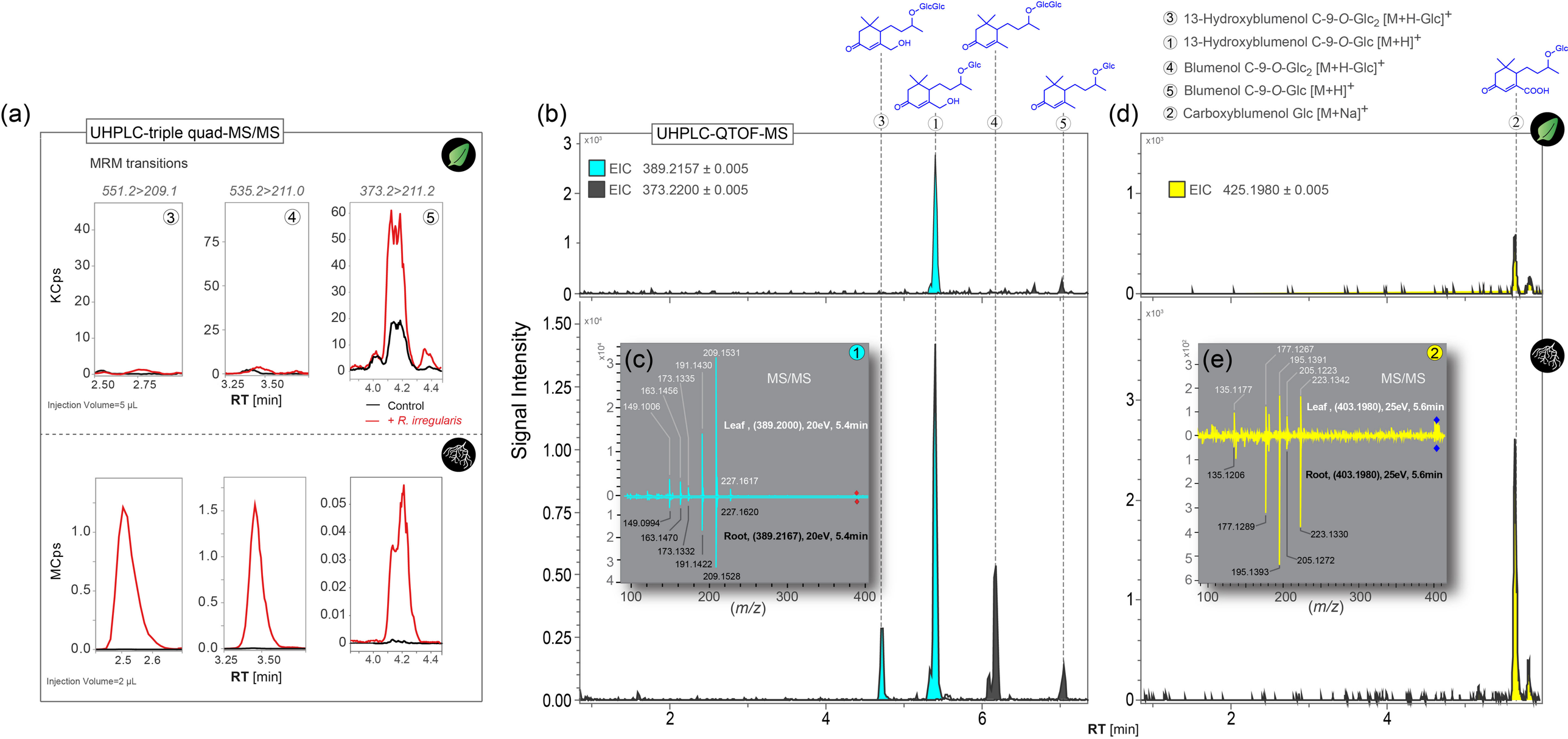
(a)
UHPLC-triple quad-MS/MS
MRM transitions
551.2>209.1
535.2>211.0
373.2>211.2
KCps
MCps
RT [min]
Injection Volume=5 µL
Injection Volume=2 µL
Control
+ R. irregularis
(b)
UHPLC-QTOF-MS
EIC 389.2157 ± 0.005
EIC 373.2200 ± 0.005
Signal Intensity
RT [min]
(c)
MS/MS
Leaf , (389.2000), 20eV, 5.4min
Root, (389.2167), 20eV, 5.4min
(m/z)
(d)
EIC 425.1980 ± 0.005
(e)
MS/MS
Leaf , (403.1980), 25eV, 5.6min
Root, (403.1980), 25eV, 5.6min
(m/z)
③ 13-Hydroxyblumenol C-9-O-Glc2 [M+H-Glc]+
① 13-Hydroxyblumenol C-9-O-Glc [M+H]+
④ Blumenol C-9-O-Glc2 [M+H-Glc]+
⑤ Blumenol C-9-O-Glc [M+H]+
② Carboxyblumenol Glc [M+Na]+

A

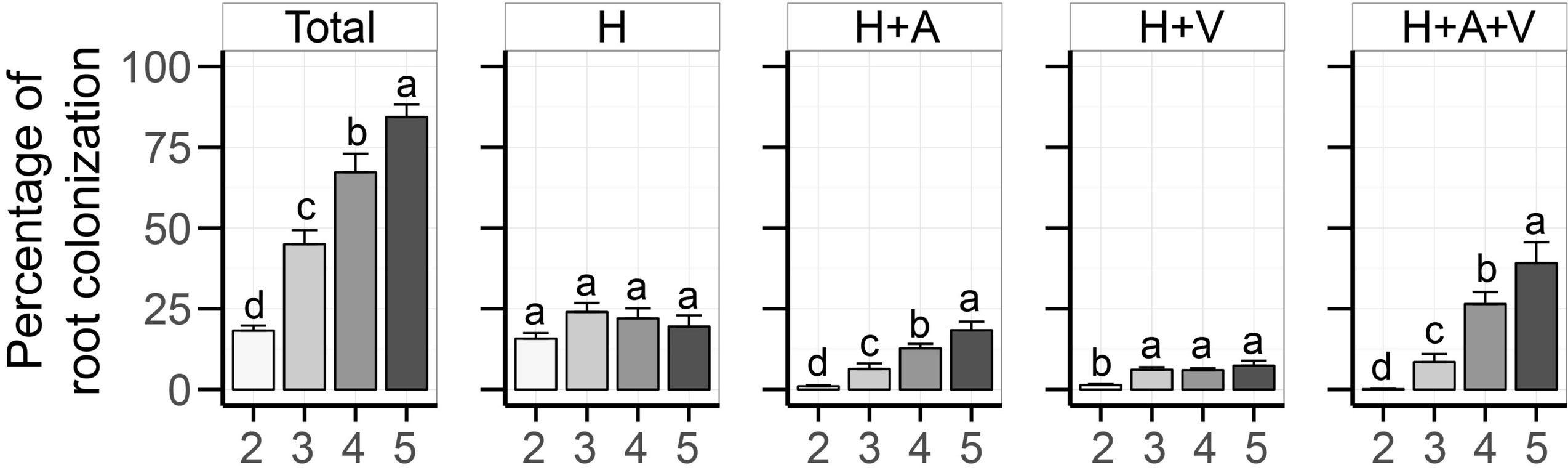

B

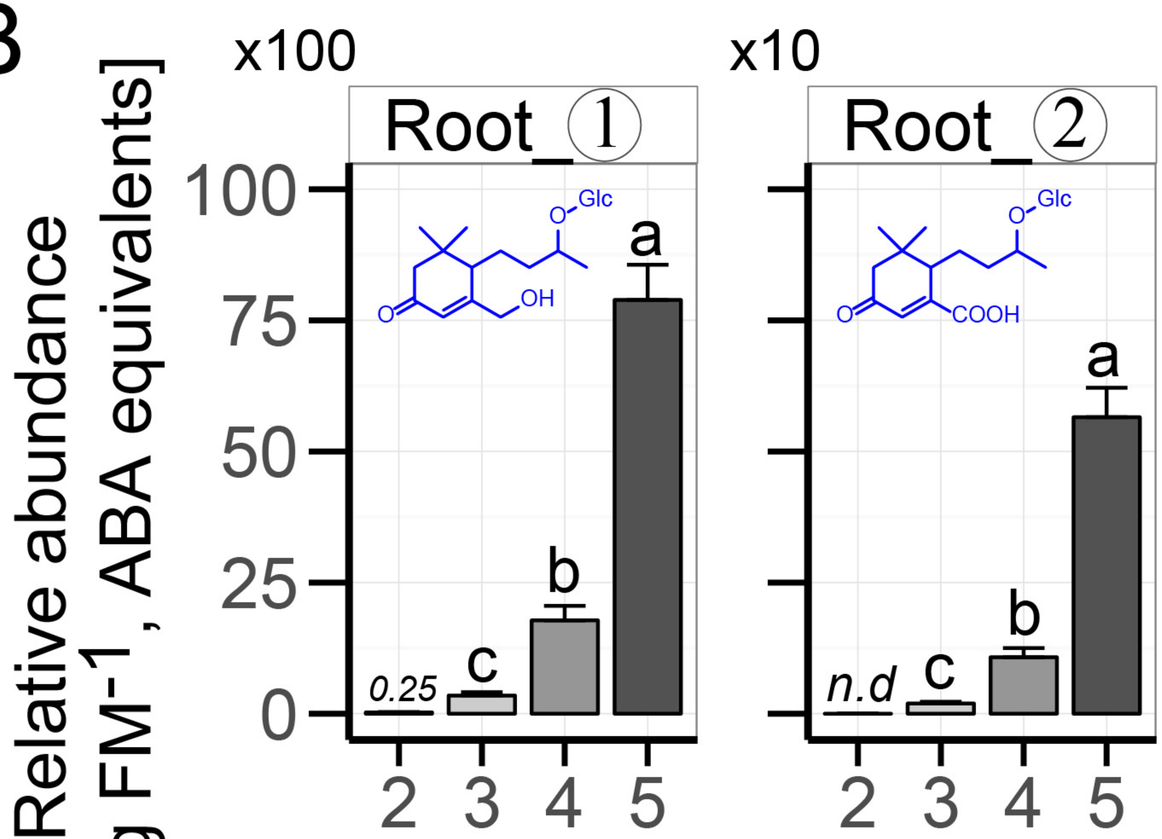

C

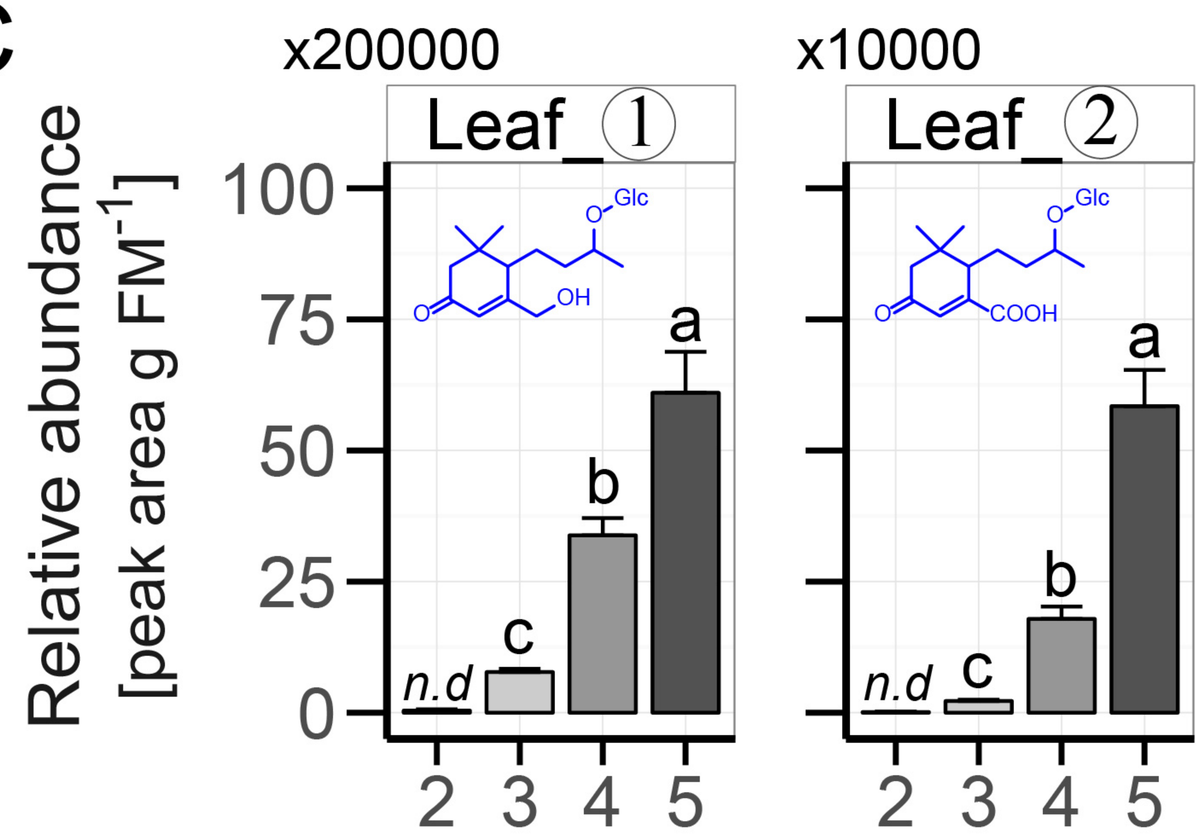

2/3/4/5 wpi (weeks post inoculation)

A

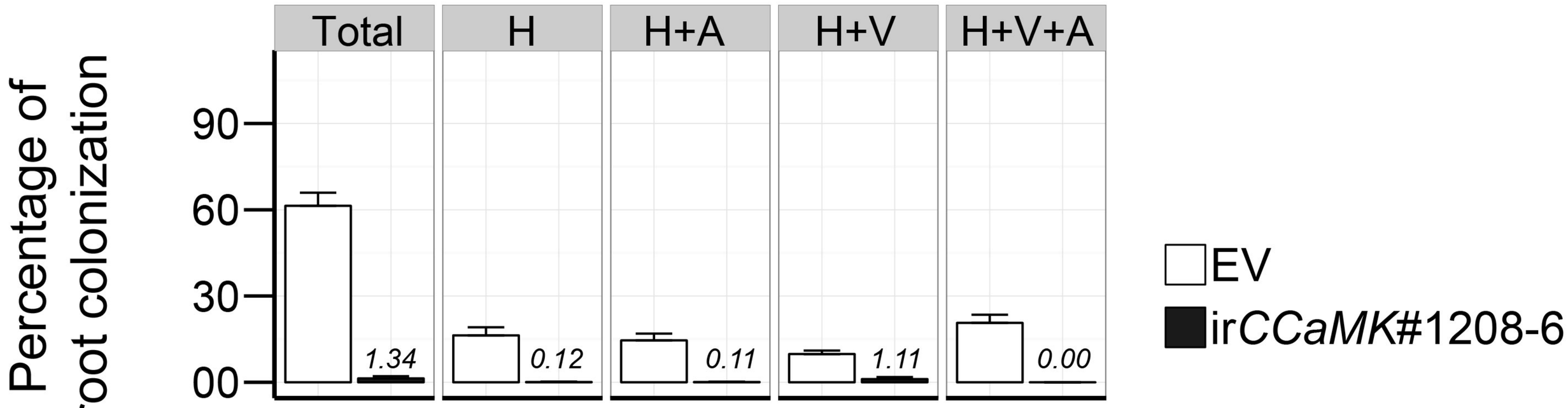
Total
H
H+A
H+V
H+V+A
Percentage of root colonization
90
60
30
00
1.34
0.12
0.11
1.11
0.00
EV
irCCaMK#1208-6

B

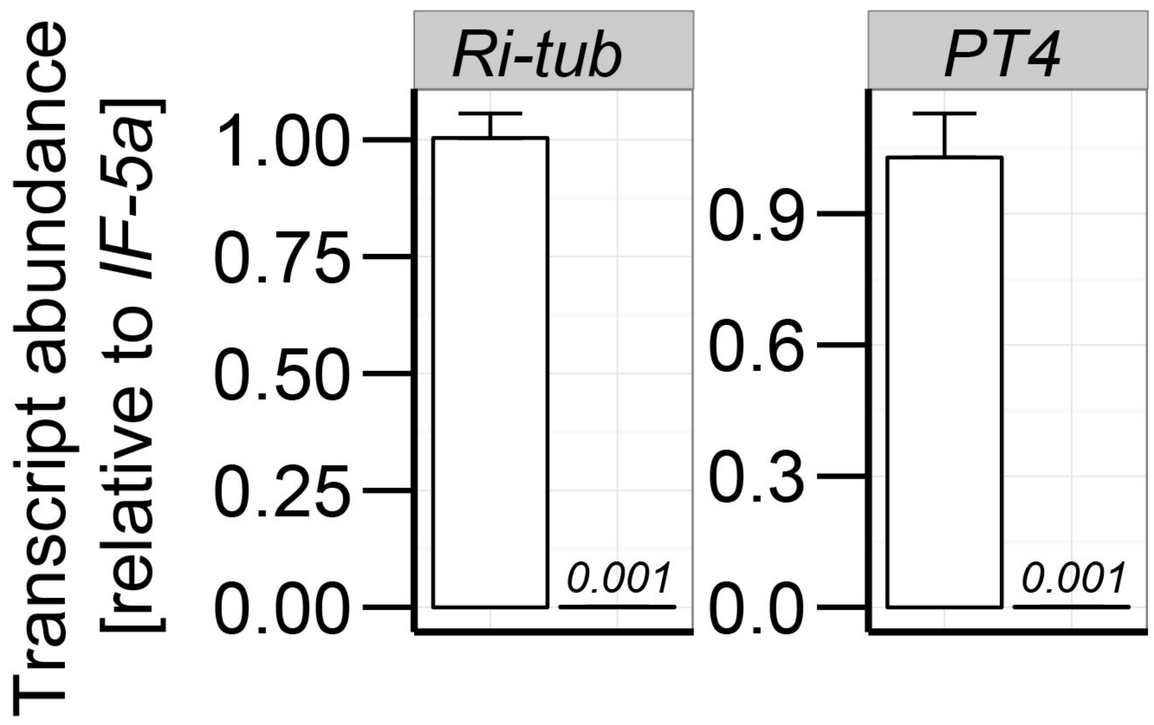
Ri-tub
PT4
Transcript abundance [relative to IF-5a]
1.00
0.75
0.50
0.25
0.00
0.9
0.6
0.3
0.0
0.001
0.001

C

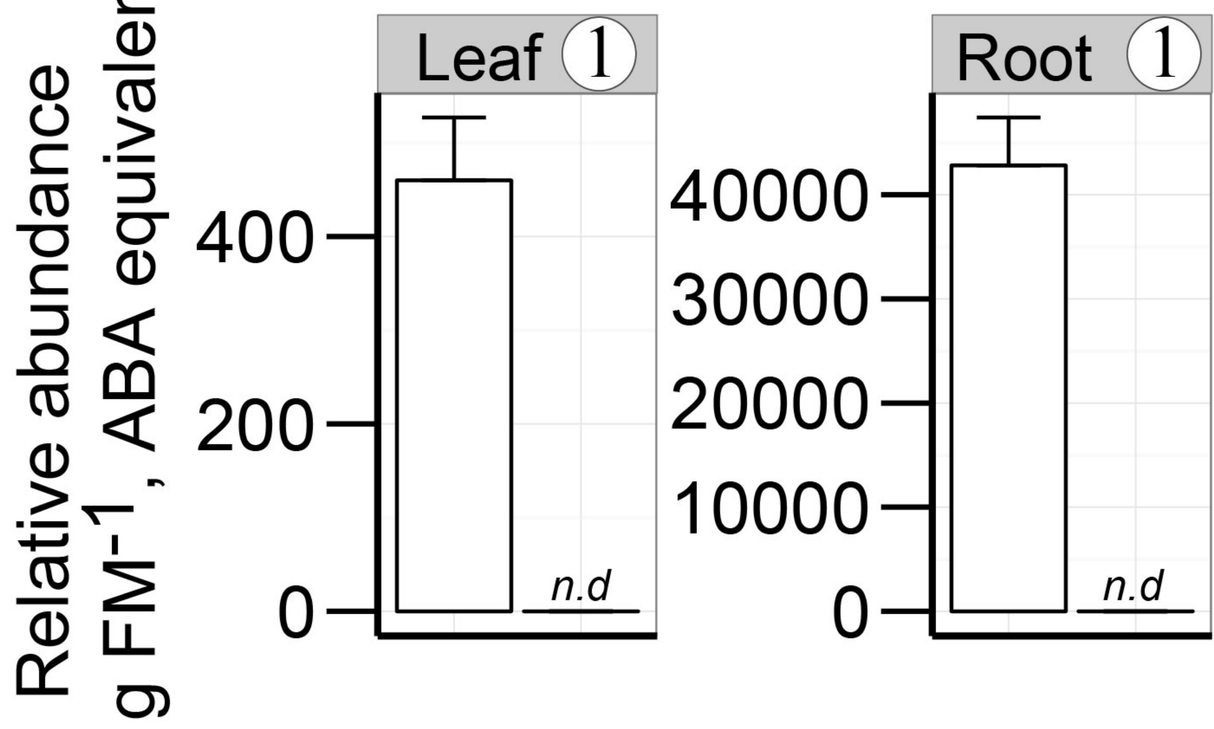
Leaf ①
Root ①
Relative abundance [ng g FM-1, ABA equivalents]
400
200
0
40000
30000
20000
10000
0
n.d
n.d

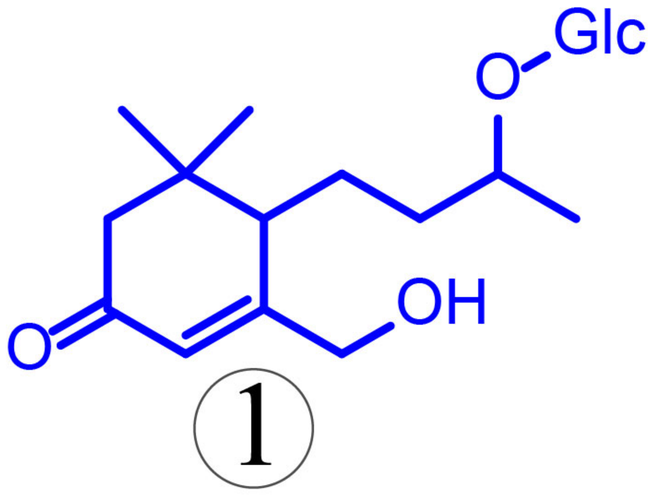

1

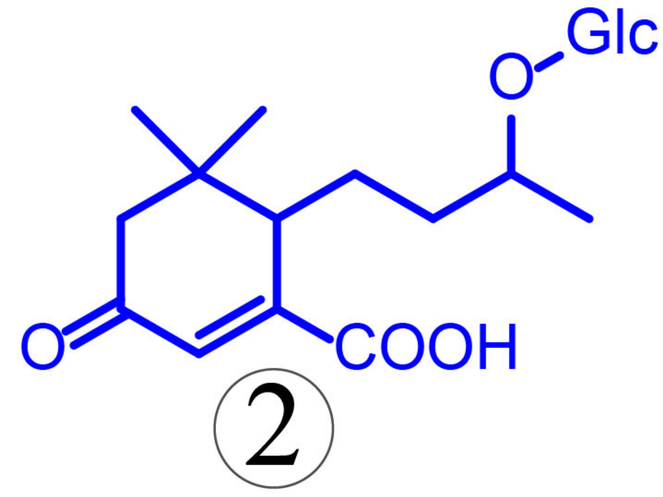

2

389.2>209.1

241.2>195.1

Signal Intensity [Kps]

Glasshouse, 2016 Field, 2016

Integration window

EV

irCCaMK

RT [min]

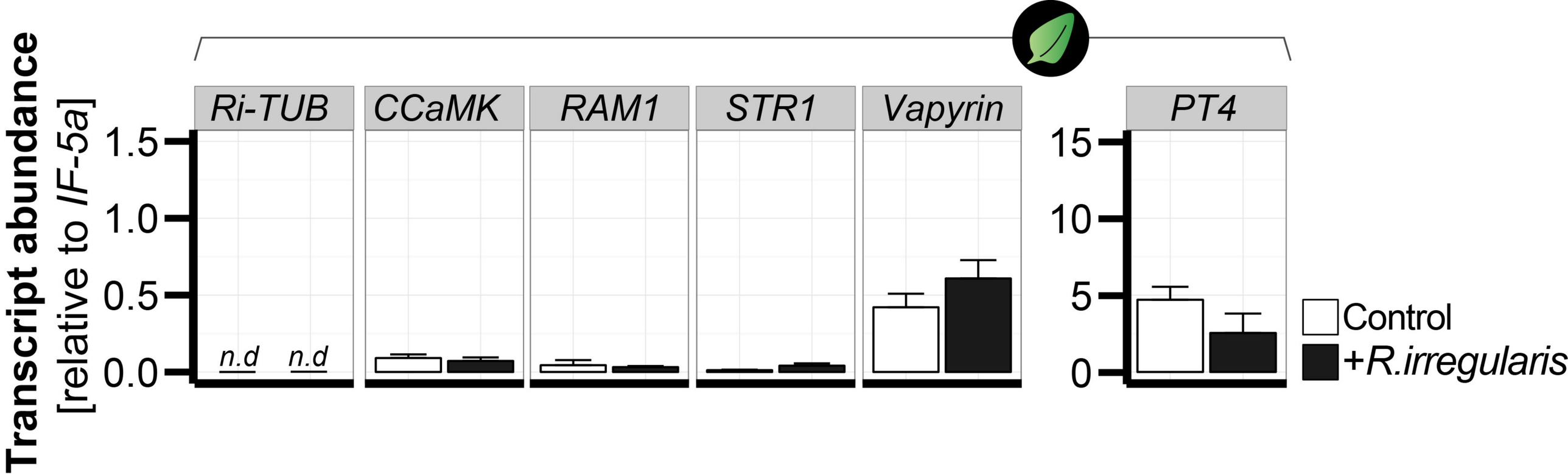
Transcript abundance
[relative to IF-5a]
Ri-TUB
CCaMK
RAM1
STR1
Vapyrin
PT4
1.5
1.0
0.5
0.0
15
10
5
0
n.d
n.d
Control
+R.irregularis

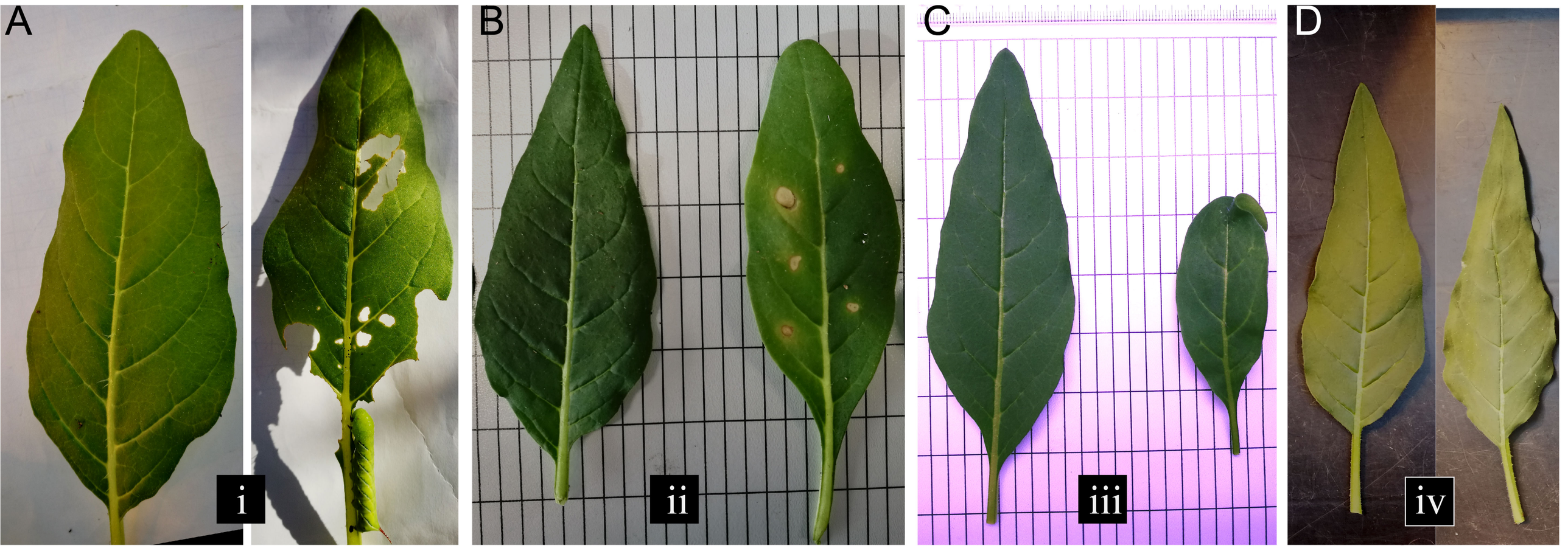

E

Treatment	Compound 1	Compound 2
i. Herbivory (*M. sexta*)	n.d	n.d
ii. Pathogen infection (*B. cinerea*)	n.d	n.d
iii. Bacteria & virus infection	n.d	n.d
iv. Drought (3 days)	n.d	n.d

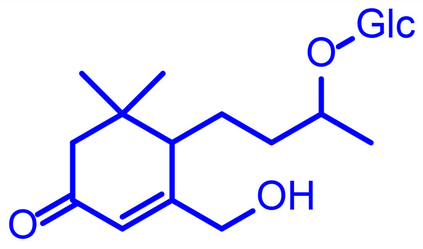

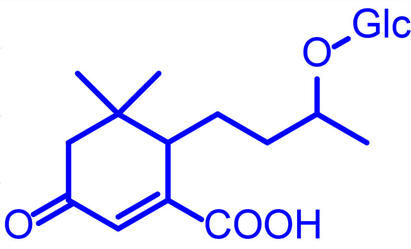

n.d, not detected

iii. Infection with *A. tumefaciens* carrying the *Tobacco Rattle Virus*

A

Fold change (log_2)

−4 0 4

Root Leaf

MAX1
D27
CCD7
PSY
CCD8
CMK
Z−ISO
MCT
CRTISO
DXS
CCD1
DXR
PDS
CYP97A3
MDS
HDS
HDR
GGPPS
LCYB

EV- EV+ irCCaMK- irCCaMK+ EV- EV+ irCCaMK- irCCaMK+

B

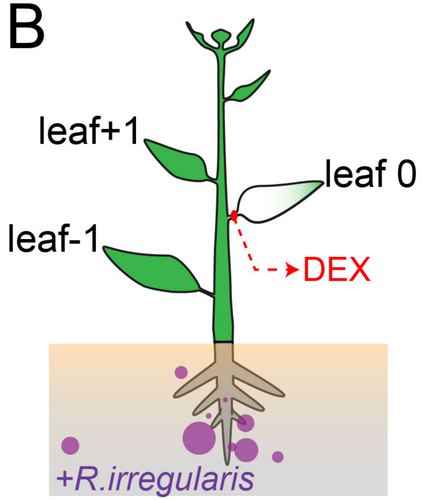

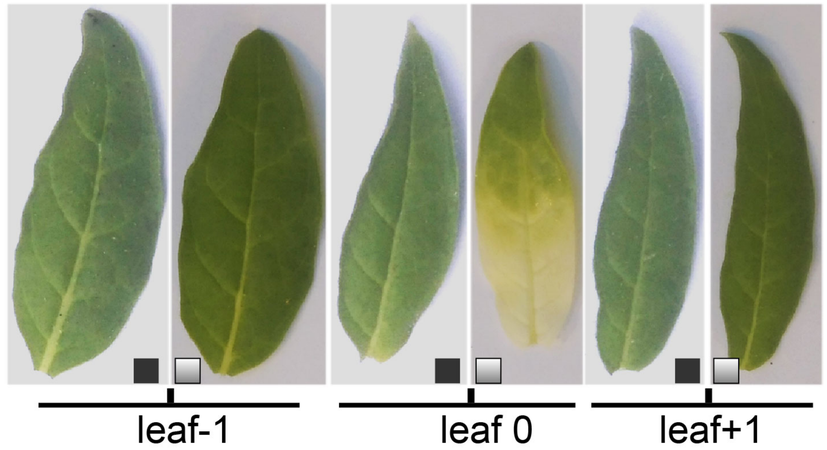

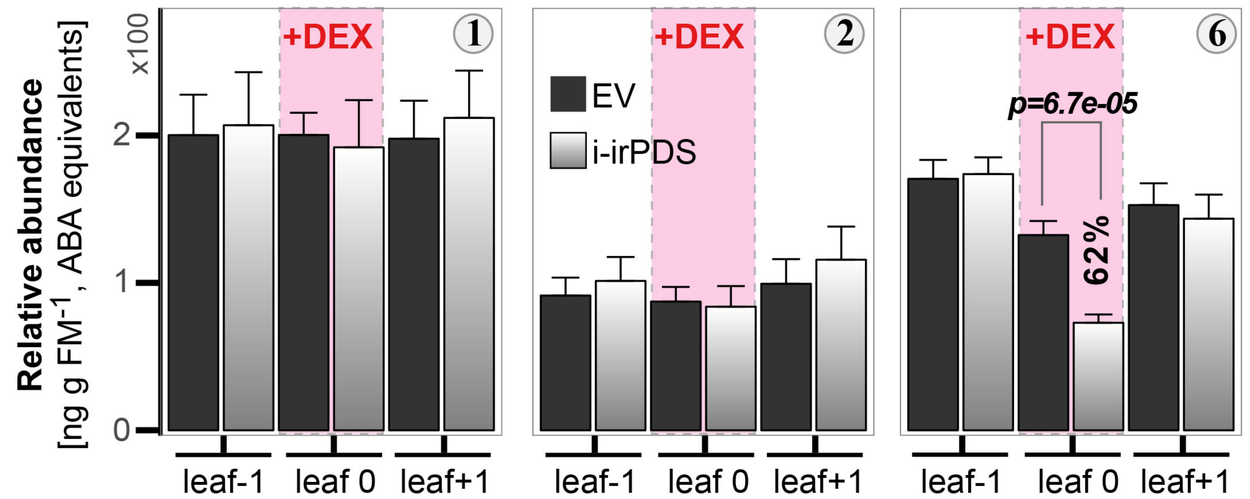

C

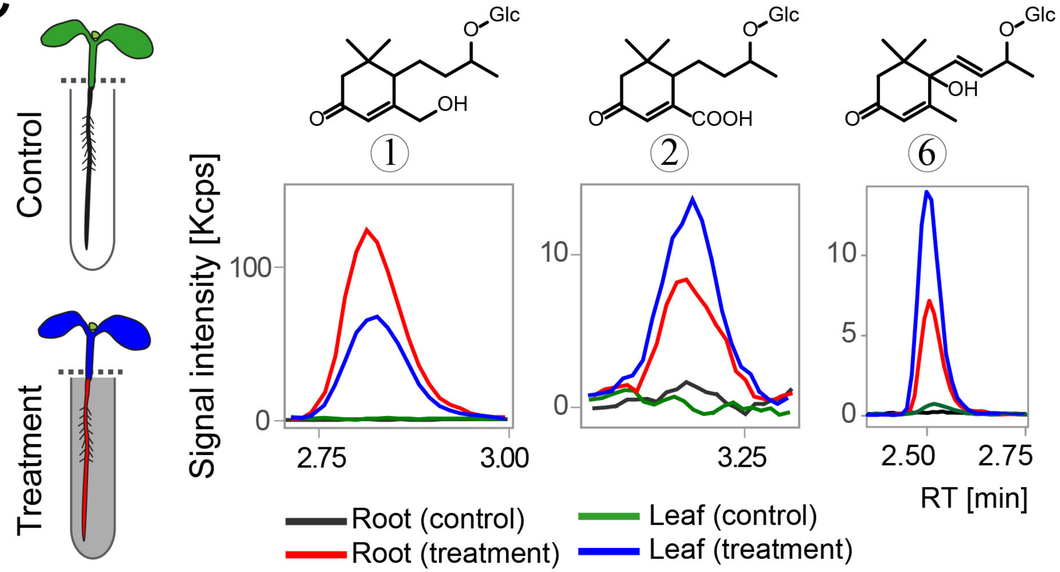

D

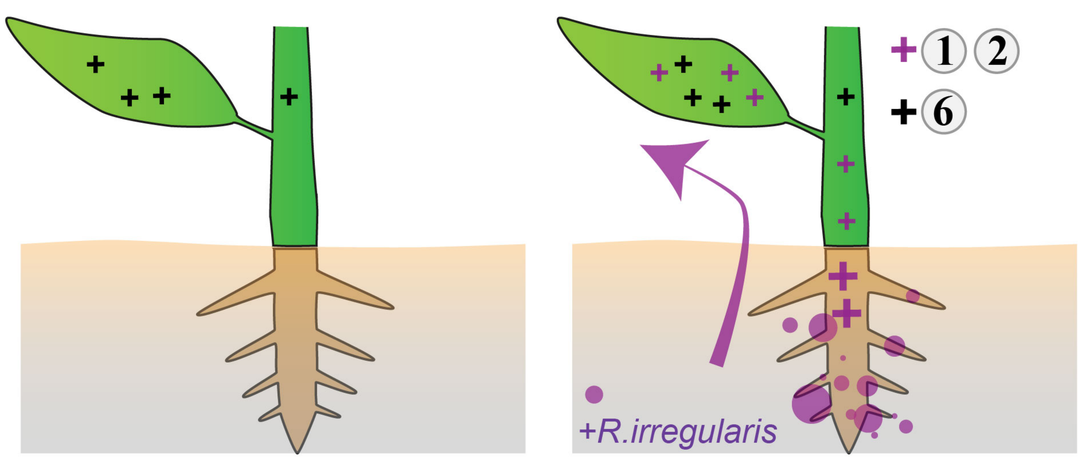

A

MEP PATHWAY

Glyceraldehyde 3-phosphate + Pyruvate

DXS

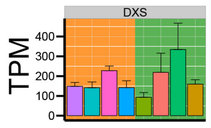

1-Deoxy-D-xylulose 5-phosphate (DXP)

DXR

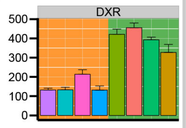

2C-Methyl-D-erythritol 4-phosphate (MEP)

MCT

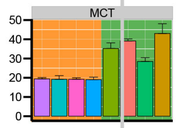

CMK

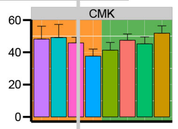

MDS

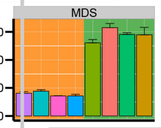

HDS

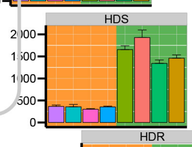

HDR

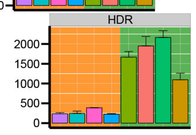

HDR

Isopentenyl-diphosphate (IPP) + Dimethylallyl-diphosphate (DMAPP)

GGPPS

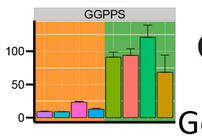

Geranylgeranyl pyrophosphate

PSY

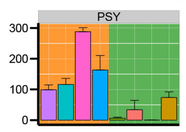

15-*cis*-phytoene

PDS

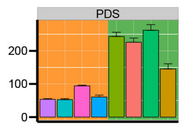

9,15,9'-tri-*cis*-ζ-carotene

Z-ISO

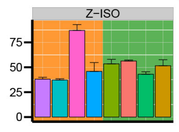

9,9'-di-*cis*-ζ-carotene

ZDS

7,9,9',7'-tetra-*cis*-lycopene (prolycopene)

CRTISO

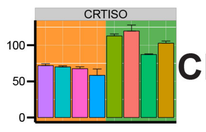

All-*trans*-lycopene

CYP97A3

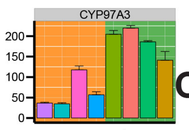

Zeaxanthin C_{40}

β-carotene C_{40}

D27

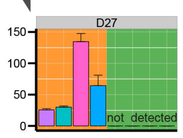

D27

9-*cis*-C_{40}

9-*cis*-C_{40}

CCD7

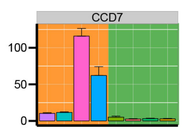

CCD7

9-*cis*-C_{27}

9-*cis*-C_{27}

CCD1

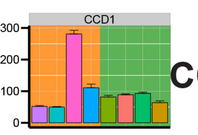

CCD8

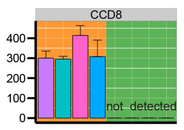

CCD8

Blumenol C_{13} + Mycorradicin C_{14}

Carlactone C_{19}

MAX1

Strigolactones C_{19}

root: EV- irCCaMK- EV+ irCCaMK+

leaf: EV- irCCaMK- EV+ irCCaMK+

B

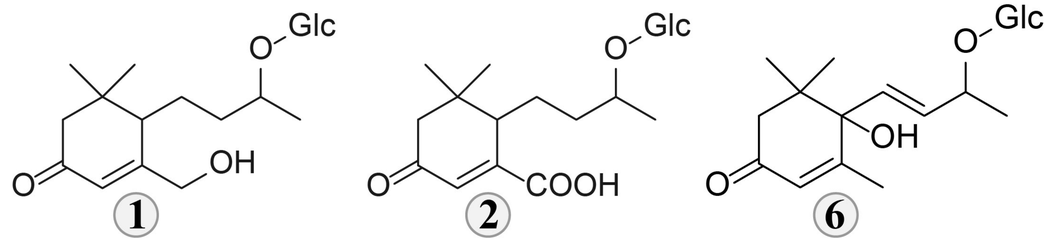

C

-R.irregularis

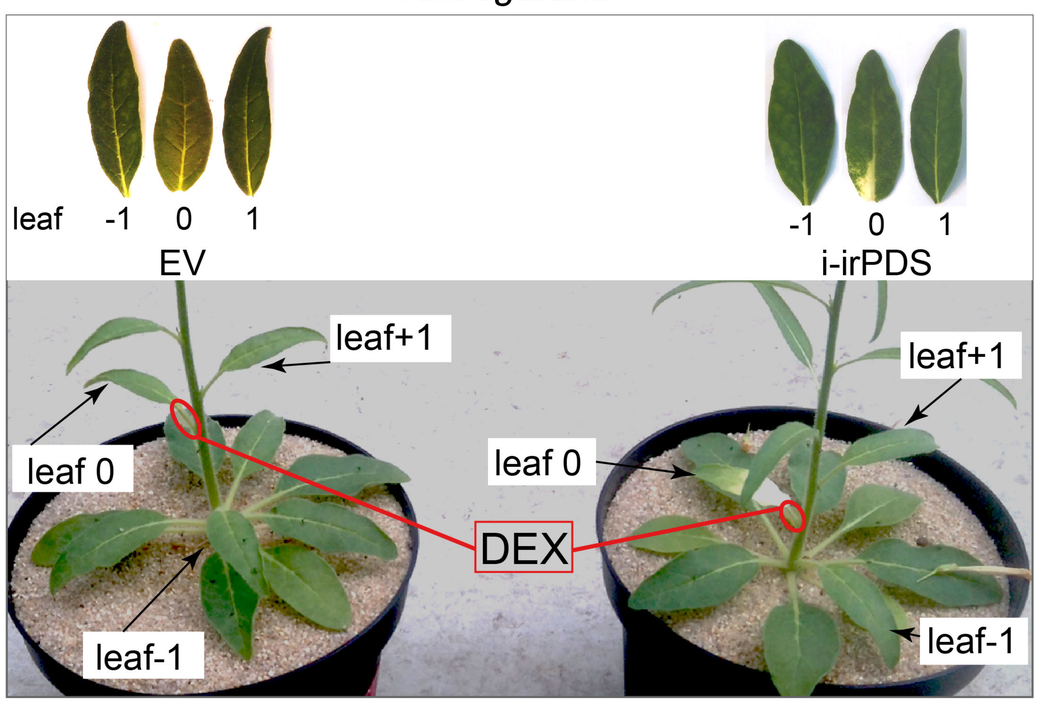

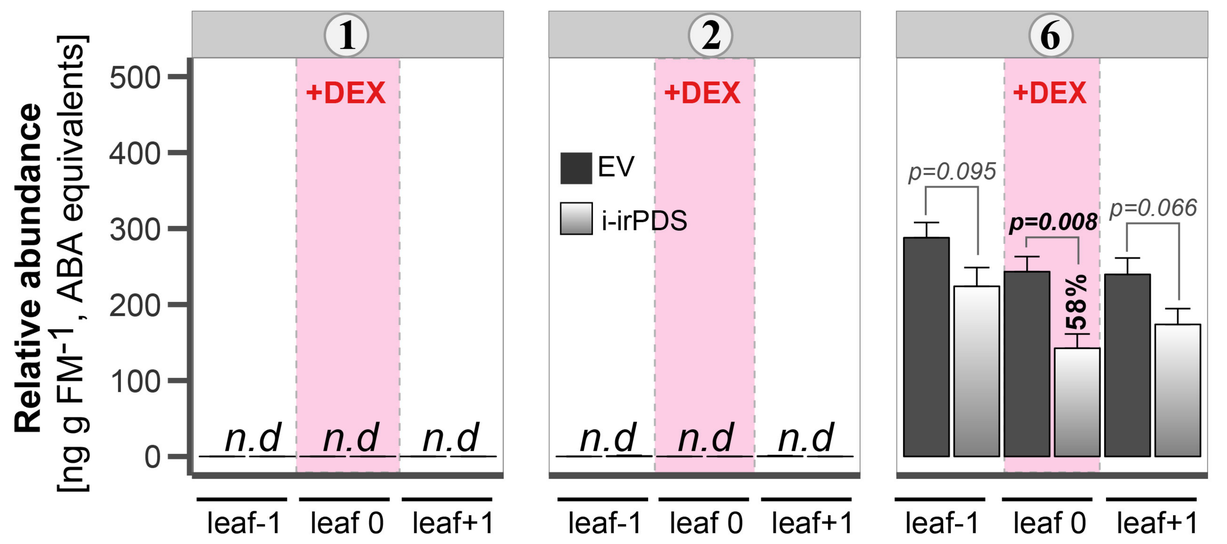

D

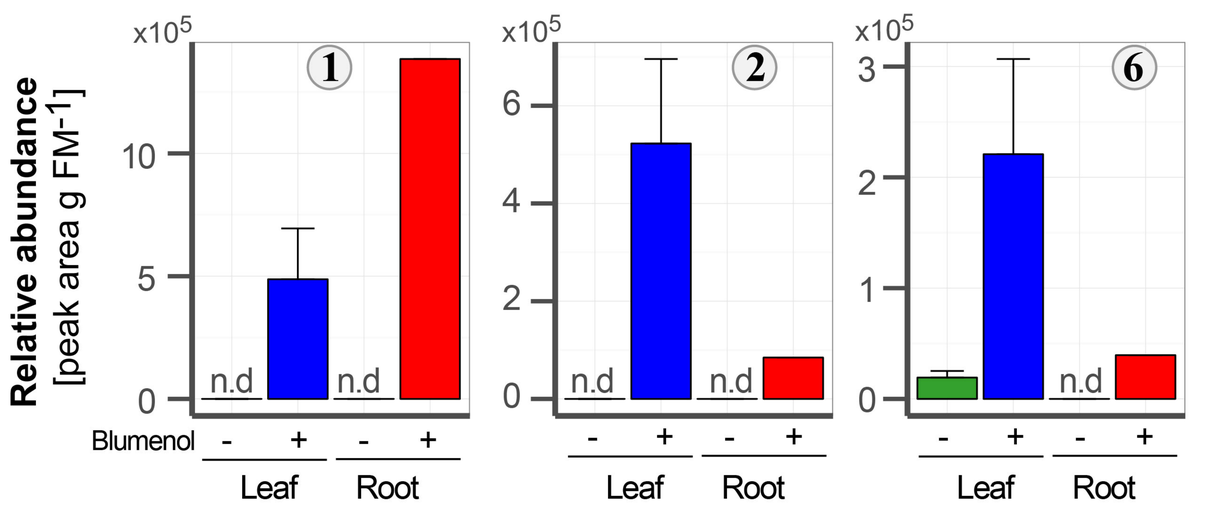

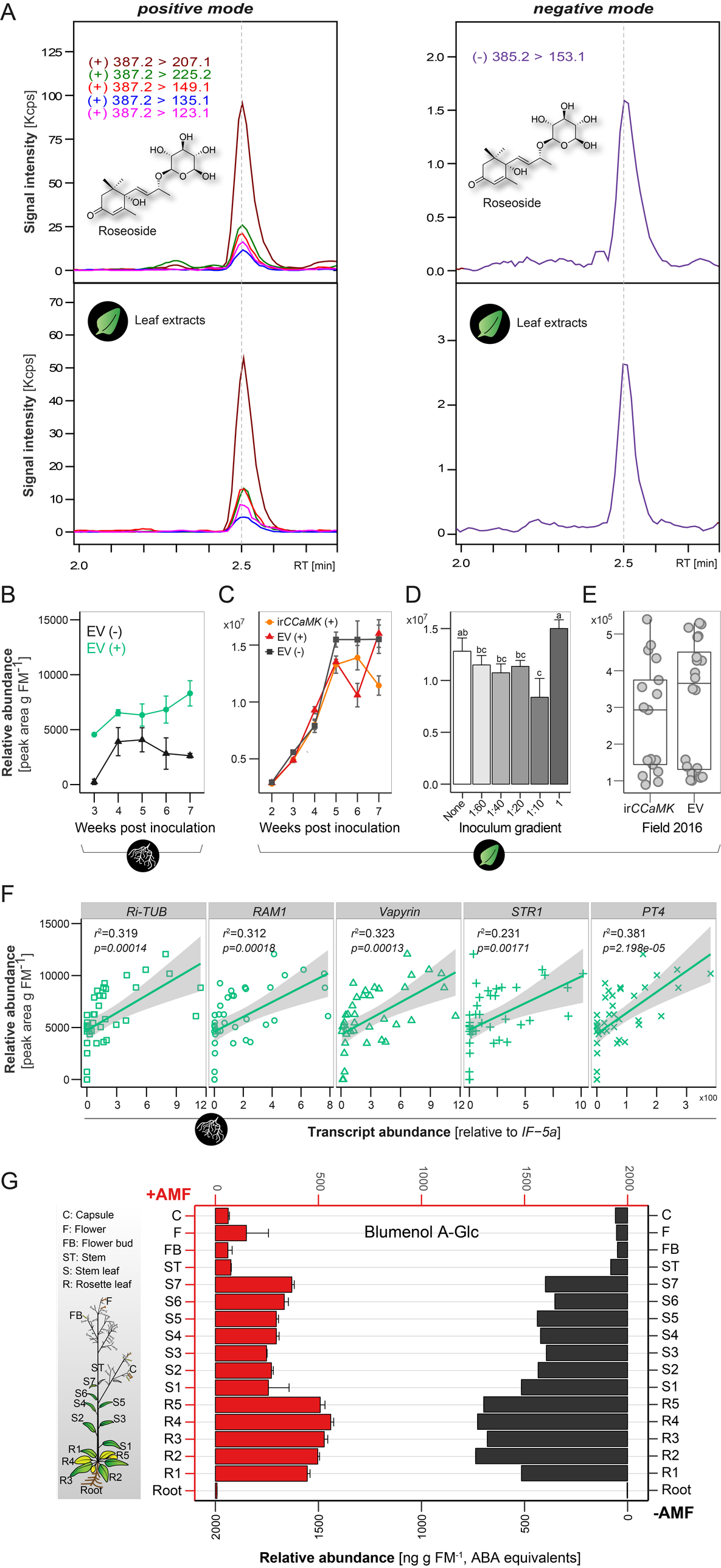
A
positive mode
negative mode
(+) 387.2 > 207.1
(+) 387.2 > 225.2
(+) 387.2 > 149.1
(+) 387.2 > 135.1
(+) 387.2 > 123.1
(-) 385.2 > 153.1
Roseoside
Leaf extracts
Signal intensity [Kcps]
RT [min]
B
EV (-)
EV (+)
Relative abundance [peak area g FM-1]
Weeks post inoculation
C
irCCaMK (+)
EV (+)
EV (-)
Weeks post inoculation
D
Inoculum gradient
None
1:60
1:40
1:20
1:10
1
E
irCCaMK
EV
Field 2016
F
Ri-TUB
RAM1
Vapyrin
STR1
PT4
r²=0.319
p=0.00014
r²=0.312
p=0.00018
r²=0.323
p=0.00013
r²=0.231
p=0.00171
r²=0.381
p=2.198e-05
Transcript abundance [relative to IF−5a]
G
+AMF
-AMF
Blumenol A-Glc
C: Capsule
F: Flower
FB: Flower bud
ST: Stem
S: Stem leaf
R: Rosette leaf
Root
Relative abundance [ng g FM-1, ABA equivalents]

A

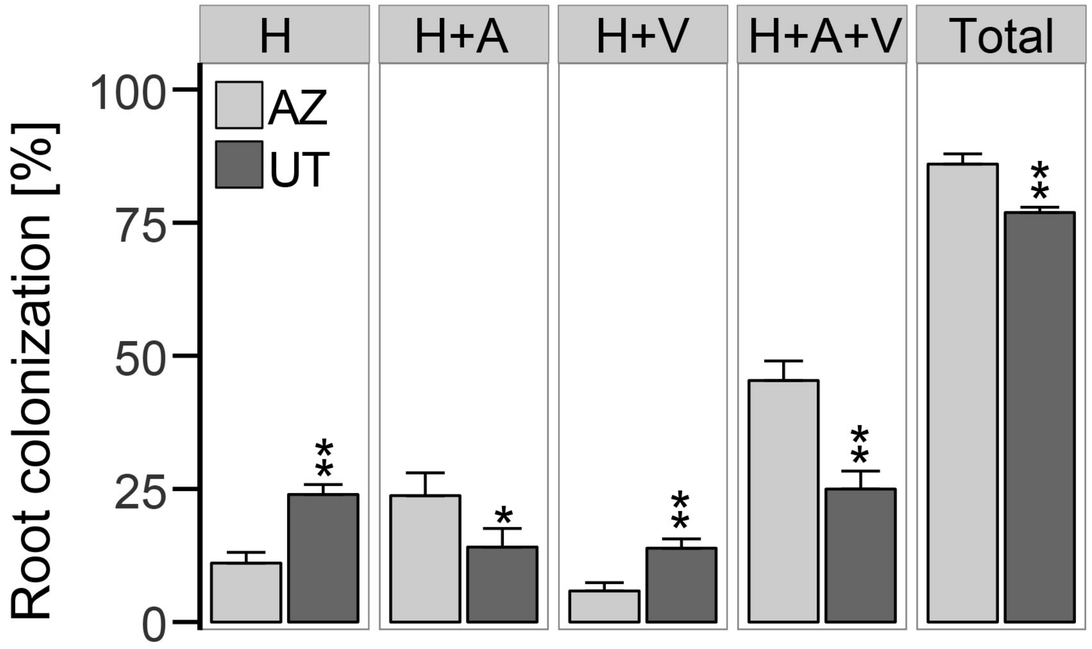
H
H+A
H+V
H+A+V
Total
AZ
UT
Root colonization [%]
100
75
50
25
0
**
*
**
**
**

B

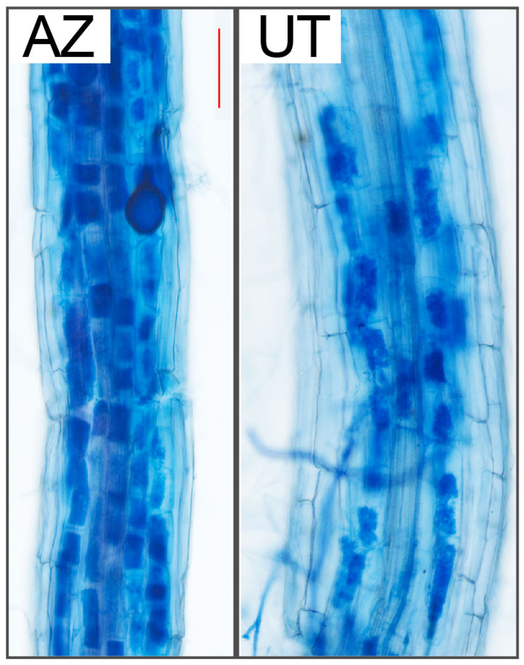
AZ
UT

C

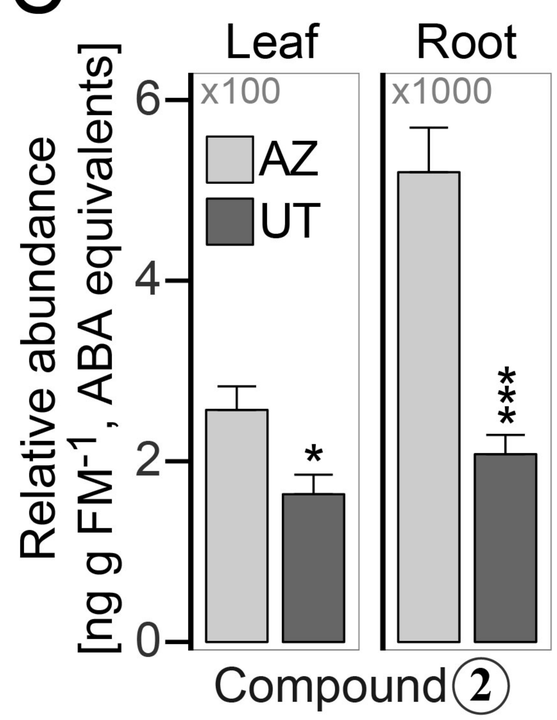
Leaf
Root
x100
x1000
AZ
UT
Relative abundance
[ng g FM-1, ABA equivalents]
6
4
2
0
*
***
Compound ②

D

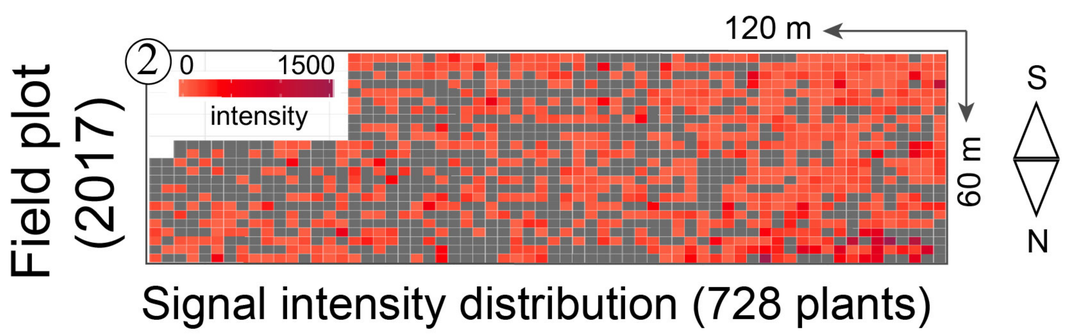
Field plot
(2017)
② 0
1500
intensity
120 m
60 m
S
N
Signal intensity distribution (728 plants)

E

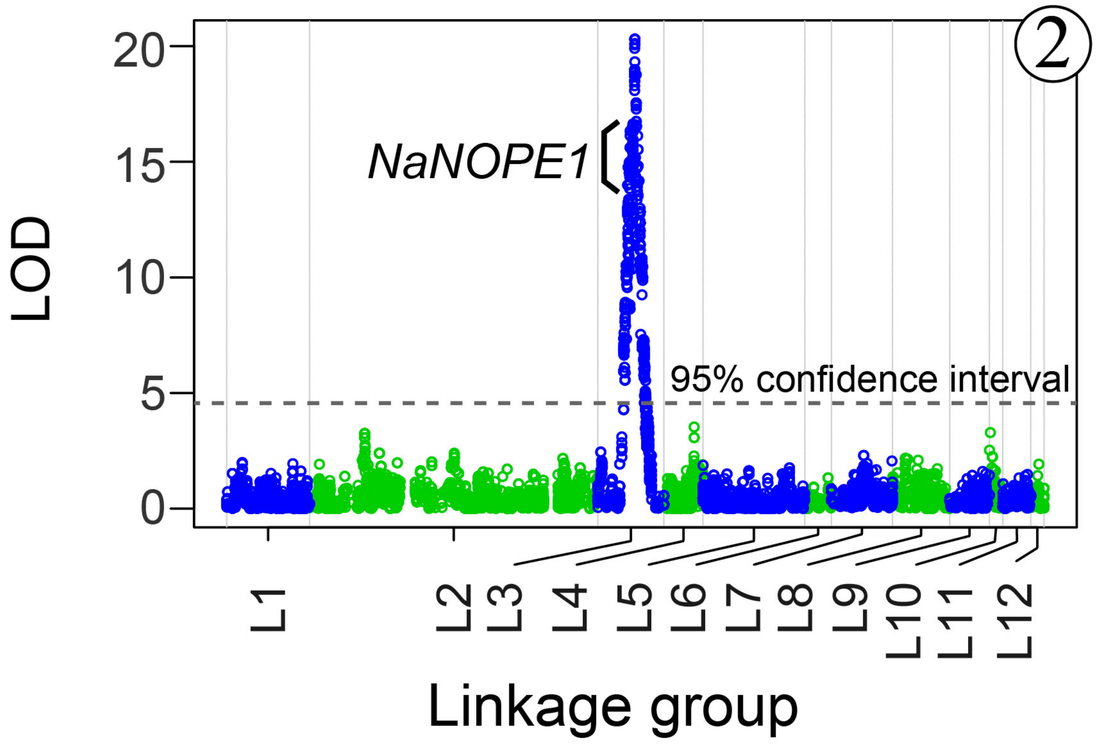
②
LOD
20
15
10
5
0
NaNOPE1
95% confidence interval
L1
L2
L3
L4
L5
L6
L7
L8
L9
L10
L11
L12
Linkage group

F

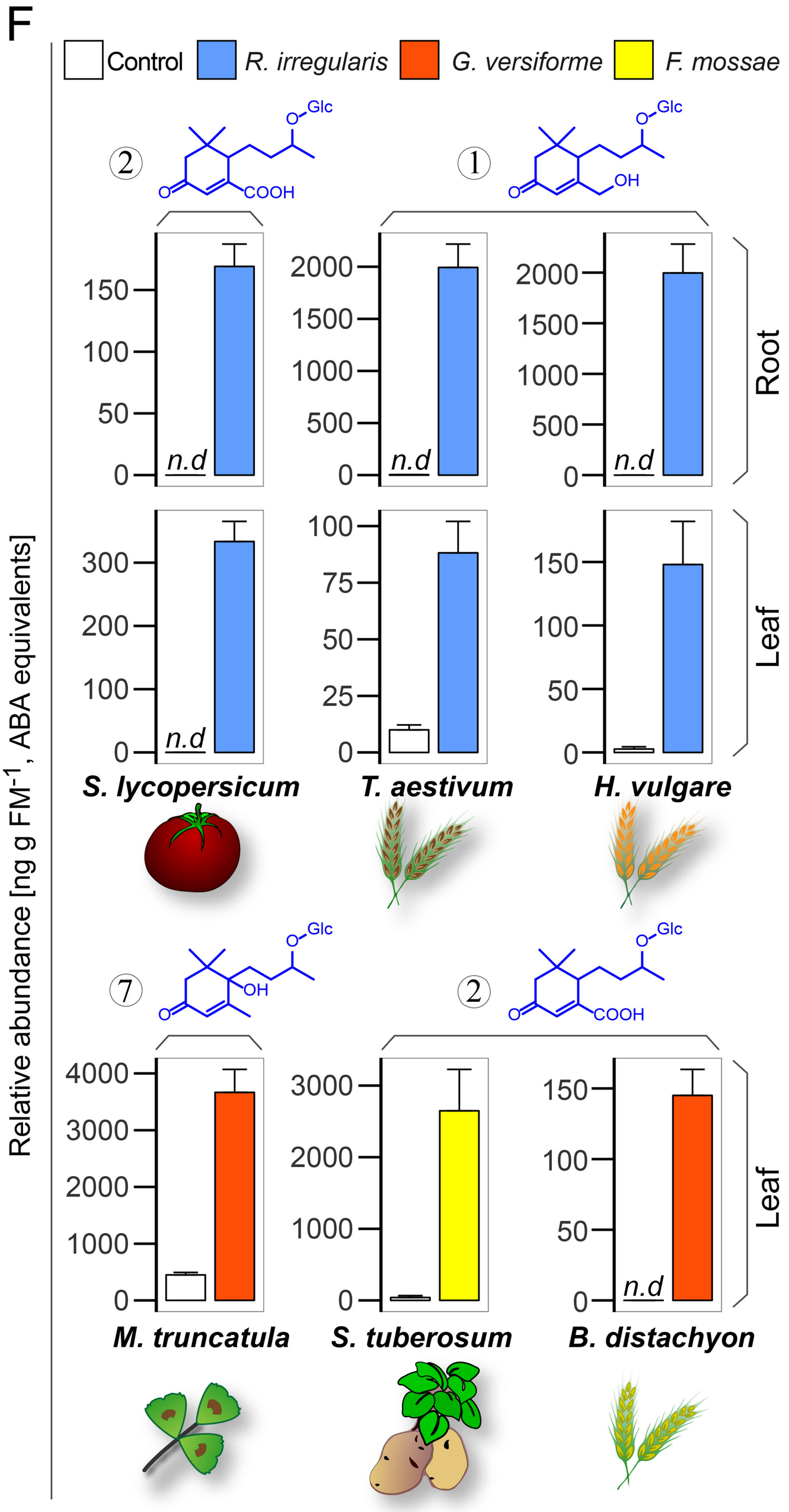
Control
R. irregularis
G. versiforme
F. mossae
Relative abundance [ng g FM-1, ABA equivalents]
② Glc COOH
① Glc OH
Root
Leaf
n.d
S. lycopersicum
T. aestivum
H. vulgare
⑦ Glc OH
② Glc COOH
M. truncatula
S. tuberosum
B. distachyon

A

B

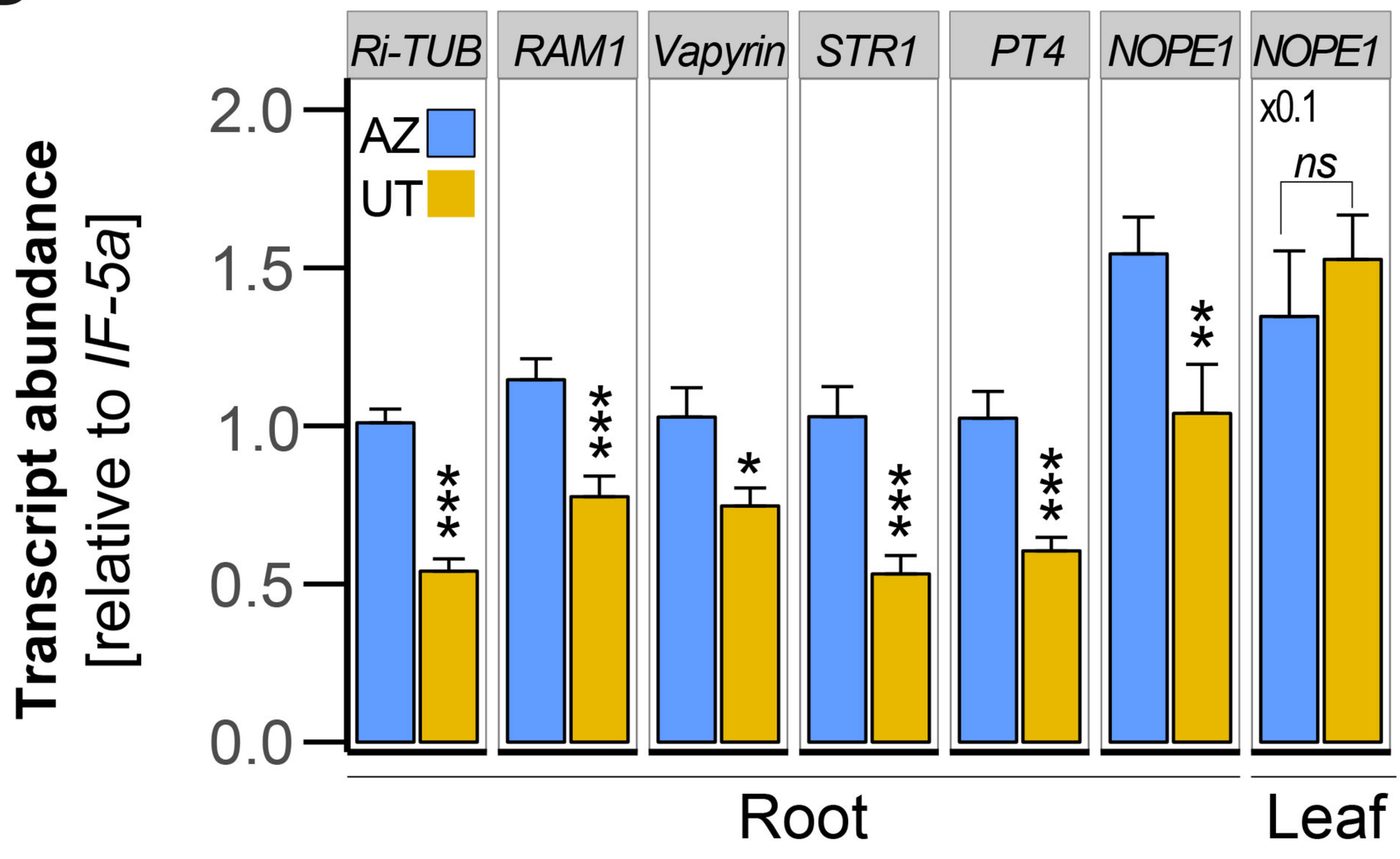

C

Field plot (2017)

(Utah, USA, N 37.1412, W 114.0275)

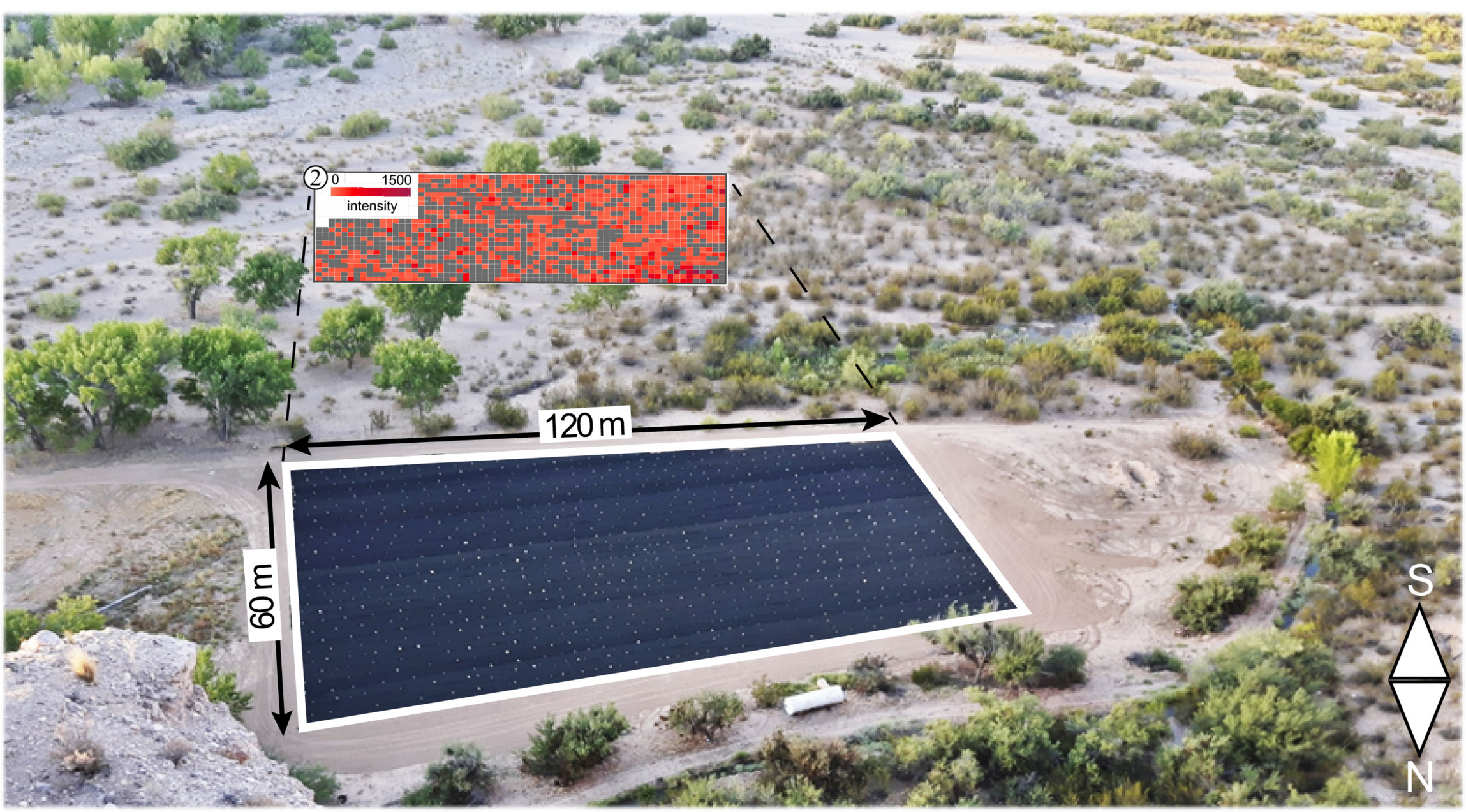

Photo by Dr. M. Schuman

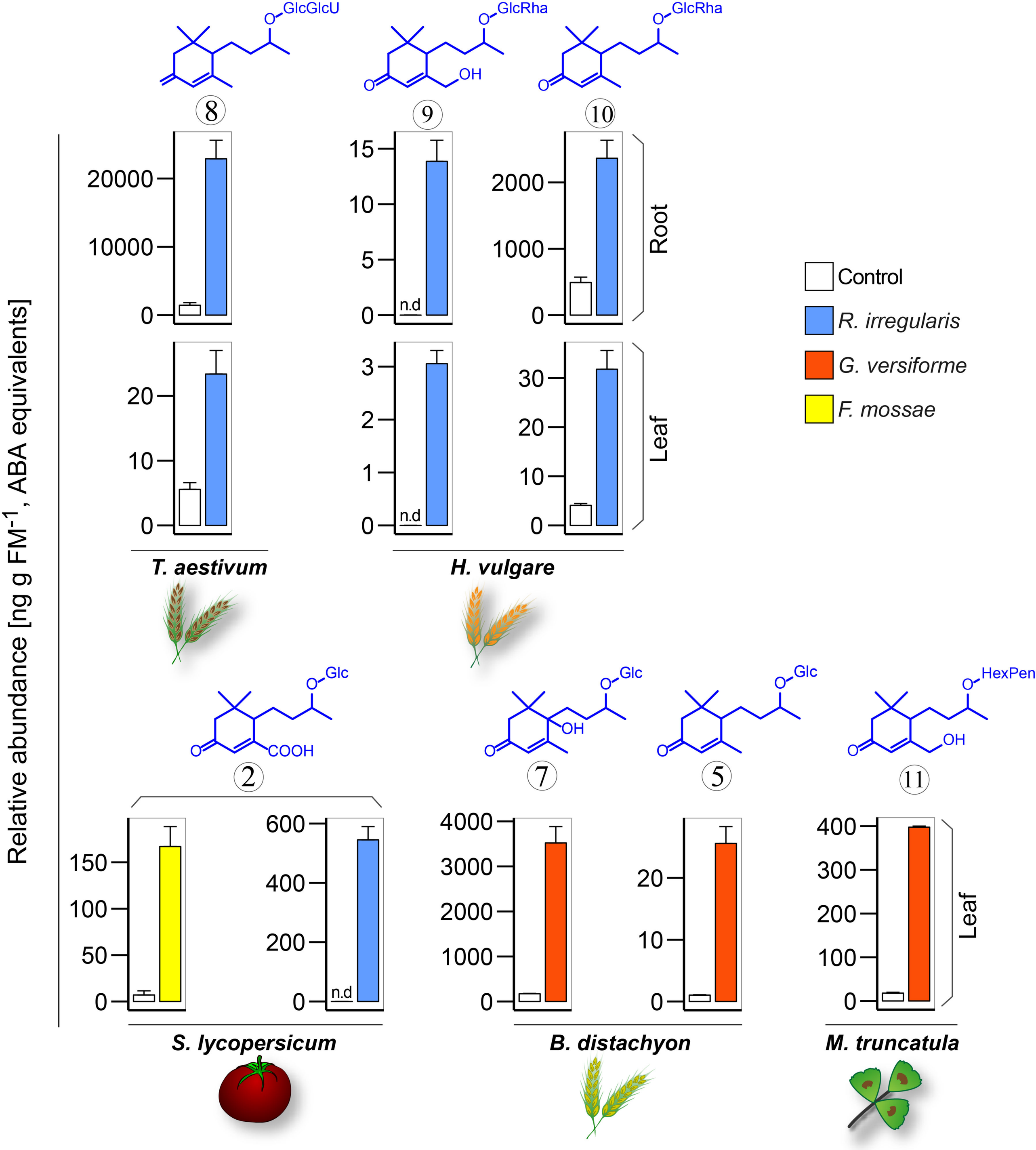
GlcGlcU
GlcRha
GlcRha
8
9
10
Relative abundance [ng g FM-1, ABA equivalents]
20000
10000
0
15
10
5
0
n.d
2000
1000
0
Root
20
10
0
3
2
1
0
n.d
30
20
10
0
Leaf
Control
R. irregularis
G. versiforme
F. mossae
T. aestivum
H. vulgare
Glc
COOH
Glc
OH
Glc
HexPen
OH
2
7
5
11
150
100
50
0
600
400
200
0
n.d
4000
3000
2000
1000
0
20
10
0
400
300
200
100
0
Leaf
S. lycopersicum
B. distachyon
M. truncatula